Trace-metal isotope 'fingerprints' of past solid Earth-ocean interactions

Markus Adloff[1,2,3], Andy Ridgwell[4], Fanny M Monteiro[1], Adina Paytan[5], and Sarah E Greene[2]

[1]School of Geographical Science, University of Bristol
[2]School of Geography, Earth and Environmental Sciences, University of Birmingham
[3]Climate and Environmental Physics, University of Bern
[4]Department of Earth and Planetary Sciences, University of California Riverside
[5]Institute of Marine Sciences, University of California Santa Cruz

March 14, 2023

Trace-metal isotope 'fingerprints' of past solid Earth-ocean interactions

Markus Adloff[1,2,3,*], Andy Ridgwell[4], Fanny M. Monteiro[1], Adina Paytan[5], Sarah E. Greene[2,*]

1 School of Geographical Science, University of Bristol, UK

2 School of Geography, Earth and Environmental Sciences, University of Birmingham, UK

3 Climate and Environmental Physics, University of Bern, Switzerland

4 Department of Earth and Planetary Sciences, University of California Riverside, USA

5 Institute of Marine Sciences, University of California Santa Cruz, USA

* corresponding authors: Markus Adloff (markus.adloff@unibe.ch), Sarah E. Greene (s.e.greene@bham.ac.uk)

Abstract

Reconstructing the solid Earth processes that impact global carbon cycling is central to a full understanding of atmospheric pCO_2 and climate evolution, both in the geological past and into the long-term future. Changes in trace-metal concentrations and isotopic compositions in ocean sediments can be read as a record of fluctuations of the solid Earth-ocean interactions we would like to better understand, because these processes often perturb metal as well as carbon cycles. However, multiple processes can affect the same trace-metal or isotope system, creating ambiguity in proxy interpretations. Taking a multi-proxy approach can help resolve this. We present an Earth system model-based systematic analysis of effects of changing weathering, sedimentation, and magmatism in multiple proxy systems (Sr, Li, Os, Ca, $\delta^{13}C$), which are critical proxy systems for unravelling the sources and sinks of carbon through time. Although different solid-Earth processes yield similar responses in individual proxy systems, each solid Earth process leaves a distinct multi-proxy geochemical 'fingerprint' in the rock record. Importantly, these fingerprints are time-dependent, often yielding more distinct responses transiently than in steady state. Finally, we show how climate and weathering feedbacks can further modulate and overprint a simpler transient response, impacting both the amplitude and timing of metal isotope excursions. Our study highlights the importance of multi-proxy approaches to studying solid Earth-ocean interactions in the geologic record and demonstrates both the benefits of fully integrating analyses of carbon and metal cycle proxy dynamics as well as the use of numerical models in disentangling coeval drivers and feedbacks.

1. Introduction

On geologically short timescales (<10,000 yr), climate is shaped by the partitioning of carbon (C) between Earth's surficial reservoirs – the terrestrial biosphere, atmosphere, ocean and surficial marine sediments. Fortuitously, changes in the partitioning of C between these reservoirs leaves a tell-tale trace as the transfer of gaseous and/or dissolved CO_2 across biological, mineral, and air-sea interfaces discriminates between the two main isotopes of C (^{12}C, ^{13}C) and hence induces a fractionation (e.g., Mook et al., 1974 and Zhang et al., 1995). Sampling the C isotopic composition ($\delta^{13}C$) of these reservoirs then provides the means to reconstruct changes in C inventories over time and potentially identify processes responsible for changes in atmospheric CO_2 and climate (Kump and Arthur, 1999). However, in such a system, an observed change in $\delta^{13}C$ cannot unambiguously indicarbonate how much C has been transferred between reservoirs or added to the system from an external source (such as from coal or natural gas), because different potential sources of C have different $\delta^{13}C$ signatures (Ridgwell and Arndt, 2015) and different quantities of C from different sources may have identical isotopic impacts. What is needed then is one or more additional proxies (measurements) reflecting unique but linked properties of the system. In this simple thought experiment, this might be radioC (^{14}C), which would distinguish between surficial C reservoirs that might have similar $\delta^{13}C$ values but very different characteristic 'ages' (e.g., soil C vs. permafrost C, Button, 1991). Or one might reconstruct changes in bulk dissolved C in the ocean from its *p*H, and hence employ a proxy such as the boron isotopic composition ($\delta^{11}B$) of carbonates precipitated from seawater (Gutjahr et al., 2017). The point is that different C reservoirs and processes moving C between them may give rise to distinct combinations of proxy responses – a 'fingerprint'.

On longer timescales (>10,000 yr), processes involving inputs (weathering, hydrothermal activity) and losses (sedimentation of biogenic minerals and organic compounds, low and high temperature seafloor alteration) of C to and from the 'solid Earth' are inevitably linked with a transfer of trace metals with their own isotopic signatures. For instance, as dissolved inorganic C (DIC) from terrestrial freshwater enters the ocean, so do metals such as calcium (Ca), silica (Si), strontium (Sr), lithium (Li) and osmium (Os), which have been dissolved from rock through corrosion by Cic and other acids (Bain and Bacon, 1994, Hu et al., 1998, Tréguer and De La Rocha, 2013, Lu et al., 2017) ('weathering'). The same applies to magmatism, which delivers C and metals from Earth's mantle to the surface. Conversely, carbonate and organic matter burial – the main mechanisms for removing C from the ocean – also constitute the primary ocean sinks for Ca, Sr, and Os. Importantly, the relative amounts of C and metals exchanged in each transfer varies and is associated with process-specific isotopic fractionations. Hence, as rates of weathering, magmatism, and sedimentation change, so do the bulk (concentration) and isotopic composition of C and metals. The formation of biogenic materials (e.g., calcium carbonate, opal, and organic matter) subsequently samples the changing marine reservoirs and, when preserved in the rock record, provides a multi-proxy reflection of surface Earth processes and potentially, a unique fingerprint of their operation.

For instance, volcanic activity associated with the emplacement of the North Atlantic Igneous province (NAIP) has been studied through a combination of C and metal isotopes

(e.g. Dickson et al., 2015, Griffith et al., 2015, Pogge von Strandmann et al., 2021). This magmatic episode is of particular interest because NAIP emplacement coincided with a large transient 'thermal maximum' warming event at the Paleocene-Eocene boundary (the 'PETM', 56 Ma) which is characterized by a pronounced negative C isotopic excursion of ca. -3‰ (McInerney et al., 2011). The combination of warming and depleted $\delta^{13}C$ values that is recorded globally in both marine and terrestrial systems suggests that C release to the ocean and/or the atmosphere drove the event. However, it remains unclear how much C was released and what specific role volcanism played. Did volcanism provide most of the C and drive most of the warming (Thomas and Bralower, 2005, Jones et al., 2019)? Did it trigger feedbacks that produced much of the warming (Kender et al., 2021)? Or did it play no significant role and the NAIP was simply coincidental to other triggers (e.g. orbital forcing, sill intrusions at continental margins) and C reservoir change (e.g. methane hydrates, Lunt et al., 2011, Reynolds et al., 2017)? The C isotope system alone is insufficient to constrain the drivers because different candidate C sources have different characteristic $\delta^{13}C$ values. Multiple combinations and sizes of C sources can then account for the PETM excursion (Vervoort et al., 2019). Adding a second C cycle proxy constraint across the PETM, e.g., for pH, then constrains the mass of C released while in theory, $\delta^{13}C$ constrains the source (Gutjahr et al., 2017). Though this method hints at a dominant role of volcanism, this still does not enable an unambiguous attribution of C sources (and hence triggers vs. feedbacks), because different mixes of C sources can be envisioned that explain the same combination of net mass and isotopic change. For example, destabilized organic C could have the same net isotopic signature and mass as a combination of biogenic methane and volcanic CO_2. Solid-Earth-process-tracing elements and associated isotopes, such as Sr, Li, Ca and Os, can be used to differentiate between these different C sources. Solid-earth tracers can also help in identifying critical processes that contributed to the excursion recovery via the removal of C (Kelly et al., 2005, Pogge von Strandmann et al., 2021, Papadomanolaki et al., 2022).

An individual trace metal proxy suffers from a similar ambiguity and cannot provide quantitative constraints on C fluxes. For instance, shifts in Sr and Os isotopes towards unradiogenic values at the PETM hint at the increased exposure of young basalt (e.g., ocean crust or flood basalts), and thus volcanic activity, or alternatively a reduction in the weathering of continental cratons (Jones et al., 2001, Tejada et al., 2009). Negative $\delta^{44/40}Ca$, $\delta^{88/86}Sr$ and $\delta^{7}Li$ shifts could have resulted from excess volcanic activity, increased land erosion, or changes in carbonate burial or secondary mineral formation rates, or a combination of these processes (Pogge von Strandmann et al., 2012, Paytan et al., 2020, Fantle and Ridgwell, 2020). In the case of the PETM, trace metal isotope interpretations even seem to contradict the lessons learned from C isotope and pH proxy analysis – radiogenic excursions of stable Sr and Os isotopes only evidence a short volcanic event and suggest that enhanced weathering of continental crust, not volcanism, was the dominant geologic control on metal cycles during the PETM (Hodell et al., 2007, Wieczorek et al., 2013, Dickson et al., 2015). This weathering event has also been identified in stable Li isotope ratios (Pogge von Strandmann et al., 2021), although it is missing from the stable Ca isotope record which instead may reflect the PETM warming (Komar and Zeebe, 2011, Kitch et al., 2021) or simply post-depositional diagenetic alteration (Fantle and Ridgwell, 2020).

The combination of different proxy systems with different ambiguities then creates its own challenge for finally deriving a fully self-consistent interpretation. Previous studies that

examined multiple trace-metal isotope systems (e.g., Misra and Froelich 2012, Pogge von Strandmann et al., 2012) addressed the complexity problem by first interrogating individual isotope mixing models in each proxy system and then combining the results. However, this approach assumes that different trace metal proxy systems are independent. Instead, some are co-dependent, that is, the environmental changes driving one proxy system may affect many others. Further, concurrent changes in C cycling and hence climate can differentially influence different trace-metal processes. While interpreting each proxy system independently is very flexible in its application, a reductionist approach cannot capture these biogeochemical links between elemental cycles, which complicarbonate a fully internally-consistent mechanistic understanding of metal and C isotope records. To guide the multi-proxy interpretation of past interactions between the ocean, atmosphere and solid Earth, we employ the intermediate-complexity Earth system model cGENIE, which incorporates representations of the global cycles of Ca, Sr, Os, Li and C and their isotopes (Adloff et al., 2021). Using this model, we simulate a series of idealized steady state and transient responses to various plausible past changes in solid Earth interactions and explore the potential for creating paleo-event ‘fingerprints’.

2. Methods

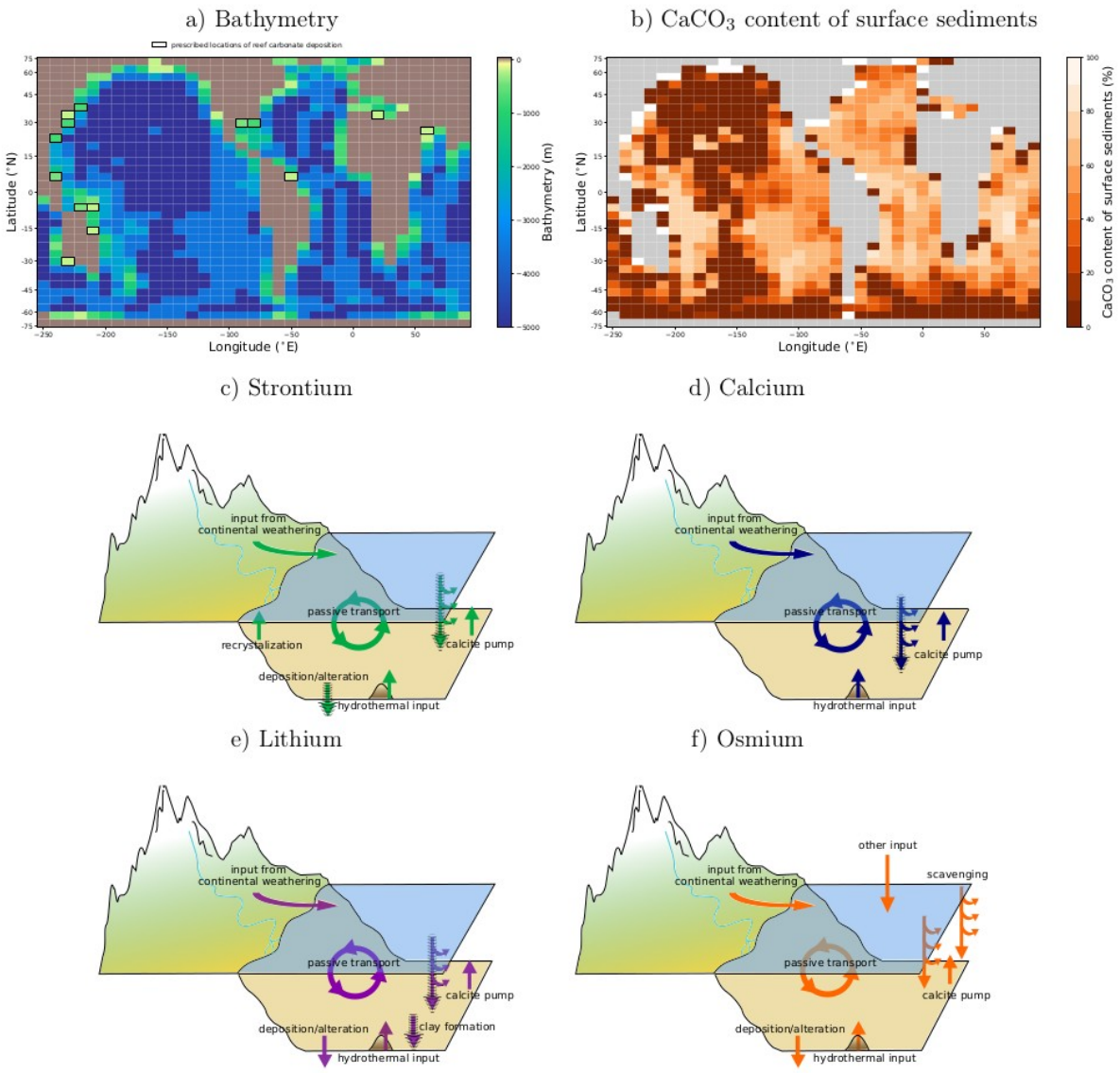

Figure 1: Pre-industrial bathymetry used in the model simulations (a), simulated baseline $CaCO_3$ content of surface sediments in pelagic and reef settings (b) and schematics of the Sr, Ca, Li and Os cycles in cGENIE (c-f). Grid cells with carbonate reefs are framed in (a). Arrows in (c-f) indicate elemental fluxes into and out of the ocean. Striped arrows indicate processes that involve stable isotope fractionation.

We used the intermediate complexity Earth system model 'cGENIE' to simulate isotopic changes in dissolved C and metals in seawater under a variety of different idealized external perturbations. cGENIE includes various marine biogeochemical cycles within the physical framework of a 3D dynamic ocean model coupled with simplified climate feedback (Edwards and Marsh, 2005) and is typically run for geological questions on a computationally efficient low-resolution grid (Figure 1). We use cGENIE combined with modules accounting for

climate-sensitive continental weathering fluxes and marine sedimentary burial and dissolution in order to account for key processes regulating ocean chemistry on geological timescales (Ridgwell et al., 2007, Ridgwell and Hargreaves, 2007, Colbourn et al. 2013). In addition to the C cycle and C isotopes (Kirtland Turner and Ridgwell, 2016), the model includes representations of the main oceanic sources and sinks of Sr, Ca, Li and Os as well as their associated main proxy-relevant isotopes that we make use of here (see Adloff et al., 2021 for a comprehensive model description and evaluation).

We make only one change here from the model setup of Adloff et al. (2021). In Adloff et al. (2021), silicate weathering contributions were split into Ca- and Mg-bearing silicates, meaning that only a part of the alkalinity supply from silicate weathering was accompanied by Ca ion input. Because climate change drives variations in silicate weathering in the model, while alkalinity is only removed in association with Ca and abyssal Mg-Ca exchange remains at a constant prescribed value (the model has no temperature-dependency for $MgCO_3$ deposition and Mg-Ca exchange at the seafloor), long-lasting perturbations could create large ion imbalances which would prevent the equilibration of the marine alkalinity and Ca reservoirs. We thus combined the climate-sensitive Ca input from weathering with the constant hydrothermal input such that all marine Ca inputs are accompanied by alkalinity inputs and that both vary synchronously with global mean surface temperature.

We ran two series of experiments using the Adloff et al. (2021) pre-industrial configuration of C and metal cycling (adjusted as described above). In the first experiment series (A), we prescribed step-changes of various boundary conditions to assess the potential of different geological processes to cause long-term shifts in the isotopic composition of dissolved metals and C in seawater. These we analysed both in terms of the final steady-state response of simulated trace-metal and isotope values, but also in terms of the non-steady-state / transient response. In the second experiment series (B), we prescribed transient external forcings taking the example of long-lasting, large-scale volcanism during oceanic plateau formation. The two experiment series are described in detail in the following sections. In both series, we refer to the relative abundances of radiogenic isotopes as isotope ratios ($^{187}Os/^{188}Os$ and $^{87}Sr/^{86}Sr$) and use the delta-notation to report stable isotope proportions ($\delta^{13}C$, $\delta^{88/86}Sr$, $\delta^{7}Li$, $\delta^{44/40}Ca$) relative to geological standard reference materials (see table 12 in Adloff et al. 2021).

2.1 Experiment series A: Fingerprints of individual solid Earth / ocean interactions

Table 1: Summary of the experiment series A simulations, presenting the range of changes in the explored processes relative to the pre-industrial setup.

Experiment name	Varied process	Range of relative changes
CO2	CO_2 outgassing	90% - 400%
CaCO3	Continental carbonate weathering rate	10% - 400%
CaSiO3	Continental silicate weathering rate	10% - 200%
WEATH	Total continental weathering rate	50% - 200%
LT-HYD	Low-temperature hydrothermal activity	50% - 200%
HT-HYD	High-temperature hydrothermal activity	50% - 400%
HYD	Total hydrothermal activity	50% - 200%
REEF	Amount of reefal carbonate burial	50% - 200%
PICPOC	Ratio of $CaCO_3$ to POC export	50% - 200%
CONG	Isotopic effect of terrestrial clay formation	0%-100%
AGE	Isotopic effect of weathering unradiogenic crust	0%-100%

Experiment series A assesses the system sensitivity to persistent changes in boundary conditions. In each of these experiments, we imposed a step change in a single parameter that controls one facet of the interaction between the ocean and solid Earth, and simulated the response of the system until equilibrium is reached. Our intention in this (focussing on individual processes in isolation), is to build up a basic understanding of the resulting proxy dynamics and explore a wide range of perturbation magnitudes. Each experiment was run for 20 Myr following the perturbation and initiated with the 15 Myr spin-up of the modern state C and trace metal cycles described in Adloff et al. (2021). We used the cGENIE model geochemical mass-balance acceleration technique (Lord et al., 2016) for increased numerical efficiency. We analysed the final equilibrium state of C and trace metals as well as and the full transient behaviour over the simulated 20 Myr interval. The chosen perturbations and associated experiments are summarized in Table 1 and described in full below.

2.1.1 CO_2 outgassing

The rate of CO_2 outgassing from the mantle to the Earth's surficial reservoirs varies over time, likely helping to sustain intervals of warm climate as well as driving pulses of transient warming (Mills et al. 2014). CO_2 outgassing impacts the marine cycling of Sr, Os, Li and Ca indirectly via climate-sensitive terrestrial inputs (weathering) and marine sediment dissolution (via the carbonate saturation control on the dissolution of calcium carbonate).

We tested the effects of four different shifts in CO_2 outgassing rates (labelled as simulations 'CO2' in Table 1, figure 2 and Table 2): 90%, 150%, 200% and 400% of the pre-industrial outgassing flux (8.57 Tmol yr^{-1}). These values span much of the range of reconstructed degassing rates over the Phanerozoic (Mills et al. 2017).

2.1.2 Continental crust weathering

Continental crust weathering is the dominant source of Sr, Os, Li and Ca to the present-day ocean, and influences surficial C cycling through CO_2 sequestration and delivery of alkalinity

to the ocean (e.g., Goddéris and Francois, 1996). The magnitude and composition of weathering fluxes is a function of climate and rock exposure, and thus can be impacted by changing climate (e.g., temperature, precipitation), as well as sea level (and changes in craton emergence), rate of mountain uplift, paleogeography, and plant productivity (see review in Penman et al. 2020). Indeed, variations in the isotopic composition of marine Sr, Os, Li and Ca reservoirs have repeatedly been used to infer past weathering fluxes and their changes over time (e.g., Hodell et al., 1990, Ravizza et al., 2001, Blättler et al., 2011, Lechler et al., 2015).

To assess the impact of weathering changes, we complemented the climate-driven weathering changes simulated in the CO_2 outgassing scenarios with non-climatically driven weathering scenarios (i.e., simple imposed changes to the weatherability of the terrestrial rock). We tested shifts of the baseline continental crust weathering rates to three different levels: 10%, 150% and 200% compared to the pre-industrial spin up. We also isolated the effects of varying carbonate versus silicate weathering rates, which have different effects on the long-term C cycle and distinct trace metal compositions, by running these experiments in three sub-series — in the first two, we changed the rates of only one of the two rock weathering types ('CaSiO3' and 'CaCO3' in Table 1) in isolation, while in the third, the weatherability of both carbonate and silicate rock are changed in tandem ('WEATH' in Table 1).

2.1.3 Hydrothermal activity

Interactions between seawater, oceanic crust, and mantle magma influence seawater trace-metal composition (e.g. Seyfried et al. 1982). Seawater can lose or gain ions in reactions with the *in situ* minerals while circulating through seafloor sediments and oceanic crust, with rates depending on the ambient temperature and geological setting. The amount of C and metals released into the ocean thus varies locally and temporally with global oceanic crust production and cooling rates and ocean temperature (Coogan and Gillis, 2018). At mid-ocean ridges, thermal springs, and other areas of volcanic activity, seawater interacts with fresh igneous material at a temperature of several hundred °C, driving elevated rates of mineral dissolution and a net flux of metals with mantle-like isotopic compositions (as well as C and heat) into the ocean (Staudigel, 2003). Away from spreading centres, dissolution rates drop off with temperature and the increasingly altered ocean crust. Yet, low-temperature ocean crust alteration also contributes to metal fluxes because of its large volume. Here, cation exchange leads to net Mg burial and Ca release (Coogan and Gillis, 2018), while Ca, Sr and Li are bound in precipitating carbonates and clay minerals from super-saturated pore waters (Schultz and Elderfield, 1997, Hathorne and James, 2006, Krabbenhöft, 2010). Sedimentary carbonates are also altered, releasing Ca and Sr into the ocean (Schultz and Elderfield, 1997, Krabbenhöft, 2010).

Rates of Sr and Li removal from the ocean in low-temperature crust alteration environments as well as Sr release from sediment recrystallization and Li supply from high-temperature processes, are all prescribed separately in the model. All other hydrothermal metal exchanges (metal release from high-temperature vents, Li removal in association with authigenic clay minerals and crust weathering) are combined into a ‘net’ hydrothermal flux to the ocean, with the assumed implicit contributions from high- and low temperature alteration

shown in Table SI.1. To explore the potential impacts on C and trace metal cycles due to changes in hydrothermal activity, we tested different changes of high- and low-temperature hydrothermal emissions separately and simultaneously (simulations 'HT-HYD', 'LT-HYD', and 'HYD', in Table 1) by varying the relevant contribution of high and low temperature processes to the net hydrothermal flux within a range consistent with estimated spreading rate variations over the past 150 Myr (Jones et al. 2001).

2.1.4 Pelagic carbonate production and burial

Biogenic carbonate production and burial dominate the removal of dissolved Sr and Ca in the modern ocean and are associated with important fractionations of the Sr and Ca (and Li) stable isotopes. From the mid Mesozoic onwards, carbonate burial has taken place both in the pelagic realm in accumulating sediments in the deep-sea, and in tropical and sub-tropical shallow water (neritic) environments (‘reefs’) (Ridgwell, 2005). The former is dominated by the preservation of carbonate shells produced by plankton, while the latter is dominated by the formation and preservation of carbonate skeletons by corals together with shells and authigenic carbonate precipitation (Sarmiento 2013, Michel 2019, Reijmer 2021). In both settings, carbonate burial removes Ca and Sr from the ocean, and, to a substantially lesser extent, Li and Os (Hathorne and James, 2006, Burton et al., 2010, Krabbenhöft et al., 2010). Sr is lost primarily in shallow water settings and associated with aragonite rather than the calcite polymorph principally produced in pelagic settings.

cGENIE includes representations of both carbonate sinks. The pelagic carbonate sink is linked to is linked to pelagic primary production in the ocean surface (Ridgwell et al., 2007a,b), while the neritic (reefal) burial is formulated as a fixed and uniform flux in shallow tropical and sub-tropical water model grid cells (figure SI.1). We explored the impact of carbonate burial changes on C and trace metal cycling independently for both settings – for pelagic carbonate burial, we tested 50% and 200% of the pre-industrial PIC:POC ratio in biogenic export from the surface ocean ('PICPOC'), simulating hypothetical changes in past changes in ecosystem structure, and for neritic (reefal) carbonate deposition (simulations 'REEF' in Table 1), rates equating to 50%, 150%, and 200% of the baseline (pre-industrial spin up) value.

2.1.5 Composition of continental run-off

For our final model sensitivity experiments in experiment series A, we explored the importance of different geochemical compositions of continental run-off, reflecting lithological, climatological, and chemical controls on the isotopic composition of terrestrial run-off rather than simply the total amount of weathered rock and/or the ratio of silicate versus carbonate weathering tested in experiments ‘CO2’ and ‘WEATH’. The isotopic compositions of dissolved Os and Sr in rivers depend strongly on the host rock’s radiogenic signature, which itself depends on the rock mineralogy and age since crystallization. Sulfide mineral-bearing and organic-rich rocks contain significantly higher concentrations of radiogenic Os than igneous rock (Esser et al. 1993, Georg et al. 2013). Similarly, the radiogenic Sr isotope ratio varies between granites, basalts and carbonates (e.g., Goldstein et al. 1988). The mineralogy of the host rock also determines its mean stable Sr, Ca and Li isotope composition (Teng et al. 2004, Tipper et al. 2008, Pearce et al. 2015). However, the

$\delta^{88/86}$Sr, δ^{7}Li, $\delta^{44/40}$Ca composition of the actual riverine input to the ocean is often dominated by the amount of dissolution and secondary mineral formation in rivers, lakes, and soils, which determine the dissolved metal load and fractionate stable isotopes (Tipper et al. 2008, Pearce et al. 2015). Changes in the spatial pattern of terrestrial weathering and hence global mean isotopic composition of runoff can, in theory, drive a marine isotopic excursion in the absence of any change in the absolute global elemental flux to the ocean or total weathering rate.

As in many metal isotope mixing models (e.g. Tejada et al. 2009, Misra et al. 2012, Blättler et al. 2011), none of these processes is explicitly simulated in the version of the cGENIE Earth system model used in the current paper. This arguably constitutes the primary simplification in all the simulations. To assess the importance of changes in the isotopic composition of continental run-off (independent of a changing climate and hence balance between carbonate and silicate weathering), we ran one set of simulations in which we first set ^{187}Os/^{188}Os and ^{87}Sr/^{86}Sr of continental run-off equal to the composition of fresh basalt ('AGE'). In a second simulation, we quadrupled the [Li] of run-off and set its δ^{7}Li composition at 2‰ to simulate a weathering regime which is fully congruent, i.e., in which all primary solutes from chemical weathering are transferred to the ocean, and terrestrial clay formation rates are minimal ('CONG' in Table 1, Misra et al. 2012). At the same time, we also set the $\delta^{88/86}$Sr to pure basaltic values to test the maximum strength of erosion- and lithology-driven changes in riverine $\delta^{88/86}$Sr (Pearce et al. 2015).

2.2 Experiment series B: Overprinting of solid Earth/ocean fingerprints by climate and C cycle feedbacks

In a second series of experiments (B), we explore the role of co-evolving climate and carbonate chemistry on trace metal cycles in response to sustained mantle emissions. The intention here is to simulate the geologic consequences of increased seafloor spreading or oceanic plateau formation and then pull this apart to elucidate the role of feedbacks for isotopic signatures in the ocean. We also use these experiments to address the question of what signals would be detected in practice in light of analytical uncertainty.

First, we elucidate the roles of co-evolving climate and carbonate chemistry on the evolution of trace-metal signatures. To do this, we run 3 experiments of total duration 5 Myr with an imposed 500 kyr long pulse of enhanced mantle input at the seafloor, followed by an unforced system recovery. For the mantle C and trace-metal input, we assumed relative abundances of C:Sr:Os:Li:Ca based on the measured present-day hydrothermal alteration of Mid-Ocean Ridge Basalts (MORB). For the first of these 3 experiments, we increased the trace-metal and C fluxes to the ocean in the model 10-fold compared to pre-industrial. To isolate the role of climate feedbacks in the evolving trace-metal inventory and isotopic composition of the ocean (and hence proxy values), we re-ran this same experiment, including the same CO_2 evolution, but with climate feedbacks disabled. With temperature and weathering now fixed in the model, only carbonate chemistry-related feedbacks – primarily the carbonate saturation controlled preservation of $CaCO_3$ at the seafloor – affect the metal systems. Finally, a third experiment was run without enhanced input of C (but still with a 10-fold tracer metal flux enhancement) and fixed atmospheric CO_2, such that neither climate nor carbonate chemistry feedbacks are induced.

Secondly, we explore which trace-metal signatures of an igneous emplacement event might be analytically identifiable in practice. We repeated the simulation above without enhanced metal inputs (only enhanced C inputs), and thus tested 3 different combinations of C vs. trace-metal enhancement –trace-metal input alone, enhanced trace-metal and C input, and enhanced C input alone. Over 1 Myr of the experiments (500 kyr of enhanced emissions, 500 kyr of recovery) we interrogated the trace-metal and isotopic composition of the ocean at time-horizons of 10, 100, 500, and 1000 kyr.

For both parts of experiment series B, results of assuming shorter durations of enhanced mantle input and additional alternative ratios of C to trace-metals are shown in SI (Table SI.1, Figures SI.5-SI.10)

3. Results

3.1 Idealized fingerprints of individual solid Earth/ocean interactions

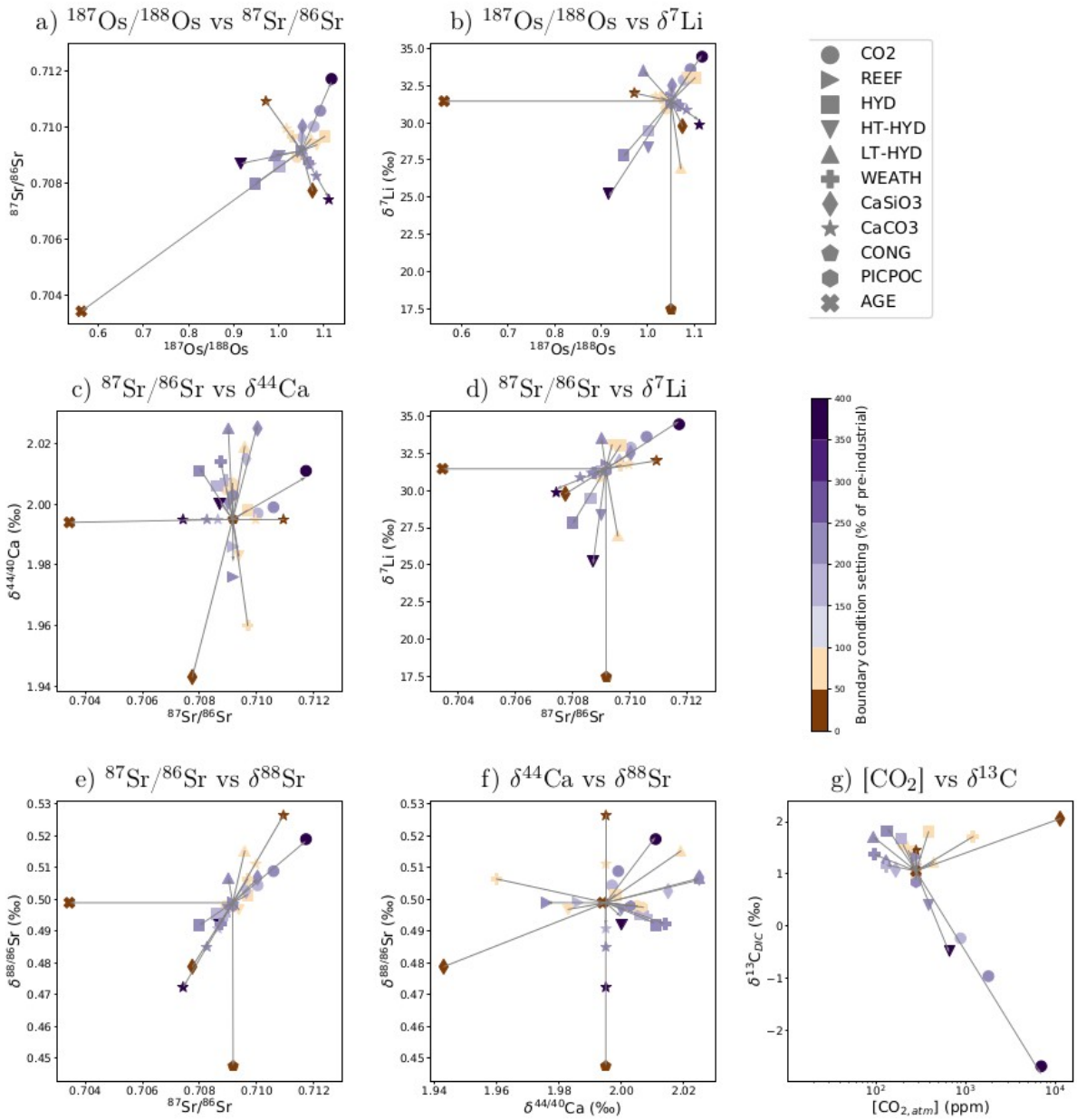

Figure 2: $^{187}Os/^{188}Os$, $8^{87}Sr/^{86}Sr$, $\delta^{88}Sr$, $\delta^{7}Li$, $\delta^{44}Ca$, $\delta^{13}C$ and atmospheric CO_2 at the end of simulations with varied solid Earth-ocean interactions of experiment series A (table 1). Every symbol style represents a different process that was changed and symbol colors indicate the different degrees of change that were tested. Arrows connect the results of simulations with the strongest forcing and the spin-up proxy value for each process, pointing in the direction of an increase in the respective condition.

We first considered the simplest, steady-state response (after 20 Myr) of seawater isotopic compositions to step changes in the processes connecting ocean and solid Earth (ensemble series A, Figure 2). In these simulations, all the changes in model processes we tested affect marine isotopic compositions, but the effects of a given process on individual isotope systems are not unique. Several processes shift individual isotopic proxies in the same direction (see also Figure SI.3), so that the direction of change in any singular proxy is not sufficient to determine which solid Earth/ocean interaction caused it. At the same time, most tested solid Earth/ocean interactions induce simultaneous shifts in multiple different isotope systems, suggesting that combining proxies might well facilitate the differentiation between various

dominant solid Earth/ocean interactions. In addition, our simulations show that the perturbation magnitude influences the amplitude of the isotopic shifts but not its direction (Figure SI.4), with the exception of changing CO_2 outgassing rates (and to a lesser extent, carbonate weathering rates) whose impact on isotopic compositions exhibits saturating behaviour at the more extreme magnitude of perturbation tested.

In general, the isotopic offset between input fluxes and the ocean determines the effectiveness of input flux changes at shifting the marine radiogenic isotope signature. Increasing the influx of radiogenic isotopes from, for example, carbonate weathering, shifts the marine isotope signature to the carbonate end member. The closer the marine isotope signature is to that end member, the smaller the impact carbonate flux increases will have. The effect of further radiogenic isotope release on marine radiogenic isotope ratios thus diminishes when terrestrial input is already very radiogenic. In the case of stable isotopes, non-linearities appear mostly under high increases of CO_2 outgassing and hydrothermal input rates, because there is an additional isotopic effect from marine burial changes on stable isotopes. In systems where metal is removed through carbonate burial, reduced carbonate burial/increased carbonate dissolution initially raise the proportion of light isotopes in the ocean, a similar effect to a larger influx of stable isotopes from the continents. As more metal accumulates in the ocean and the carbonate system rebalances through sedimentary burial, metal burial fluxes increase too, eventually matching additional inputs. During this phase, stable isotope fractionation from increased metal burial shifts the marine stable isotope ratios away from the lighter continental end member.

Table 2: Atmospheric CO_2 and seawater composition changes as a result of variations in process strength in experiment series A applied to the pre-industrial model set-up. The table presents isotopic and concentration shifts from the most extreme boundary changes that we tested (see Table 1). Negative and positive changes outside of measurement uncertainty are highlighted in blue and red, respectively. Colour shading indicates the scale of the change relative to the maximum change across all simulations.

Simulation \ Proxy	$^{187}Os/^{188}Os$	$^{87}Sr/^{86}Sr$	$\delta^{88}Sr$ (‰)	$\delta^{7}Li$ (‰)	$\delta^{44/40}Ca$ (‰)	$\delta^{13}C$ (‰)	CO_2 (ppm)
CO2 -10%	=	-0.0002	-0.01	-0.33	-0.02	+0.45	-77.0
CO2 +300%	+0.06	+0.0024	+0.02	-7.16	-0.02	-3.62	+5685.0
HYD -50%	+0.05	+0.0006	+0.02	+2.46	+0.01	=	+102.0
HYD +100%	-0.11	-0.0013	-0.03	-3.67	-0.04	-0.14	-147.0
HT-HYD -50%	+0.03	+0.0002	=	+1.62	-0.01	+0.4	-47.0
HT-HYD +100%	-0.14	-0.0005	+0.02	-6.8	+0.04	-1.63	+351.0
LT-HYD -50%	+0.02	+0.0004	+0.02	-4.53	+0.02	=	+161.0
LT-HYD +100%	-0.02	-0.0003	=	-0.13	-0.03	=	-124.0
WEATH -50%	-0.02	+0.0005	=	+0.25	-0.04	+0.43	+933.0
WEATH +100%	+0.02	-0.0004	=	-0.27	+0.02	-0.15	-183.0
CaSiO3 -50%	+0.01	-0.0003	=	-0.1	-0.02	+0.32	+933.0
CaSiO3 +100%	-0.02	+0.0005	=	+0.16	+0.03	=	-183.0
CaCO3 -90%	-0.08	+0.0018	+0.03	+0.55	=	+0.42	=
CaCO3 +300%	+0.06	-0.0017	-0.03	-1.59	=	-0.21	=
REEF -50%	=	=	=	-0.14	=	-0.13	=
REEF +100%	=	=	=	+0.29	-0.02	+0.27	=
PICPOC -50%	=	=	=	-0.11	+0.01	=	=
PICPOC +100%	=	=	=	-0.16	=	-0.15	=
CONG 100%	=	=	-0.05	-14.0	=	=	=
AGE 0%	-0.49	-0.0057	=	=	=	=	=

We summarize these steady-state isotopic shifts in Table 2, indicating the largest amplitude simulated for each tested process. No two perturbed processes showed shifts in the same directions in all isotope ratios and atmospheric CO_2 at once, except decreased reef carbonate deposition and increased PIC:POC of pelagic primary production, which effectively both result in a net increase of pelagic carbonate burial and only had an meaningful (but still very minor) impact on δ^7Li and δ^{13}C. Hence, most tested process changes result in a unique isotopic and C cycle 'fingerprint' when all proxy systems are considered. This means that changes in different mechanisms of solid Earth-ocean exchange could in theory be distinguishable in the geological record through the combined evidence of excursions in multiple metal and C isotope systems.

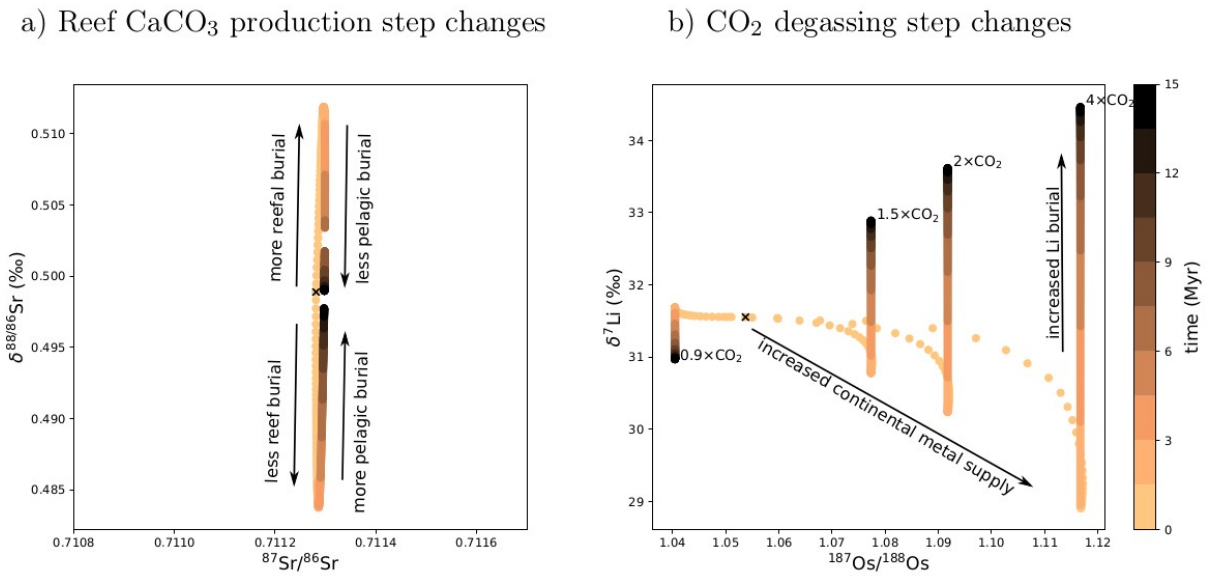

Figure 3: Competing isotopic effects in the transient response to step changes in two boundary conditions in ensemble A. a) δ^{88}Sr and ^{87}Sr/^{86}Sr variations due to increased and reduced carbonate deposition at reefs ('REEF' experiments). b) Evolution of δ^7Li and ^{87}Os/^{188}Os under increased and reduced CO_2 degassing ('CO2' experiments).

There is another dimension to trace-metal fingerprints however. As demonstrated in a recent model-based analysis of ^{87}Sr/^{86}Sr and $\delta^{88/86}$Sr trends by Paytan et al. (2021), the final steady state shifts tend to be much smaller than the shifts observed during the equilibration phase. In Figure 3, we show as example how four isotopic proxies (radiogenic vs stable Sr isotopes and radiogenic Os vs Li isotopes) respond to perturbations in reefal carbonate burial and CO_2 outgassing over the equilibration period (from 0 to 15 Myr after the perturbation). Each dot represents the mean ocean isotopic composition at a specific time following the perturbation, with advancing time indicarbonated by darkening colors. In Figure 3a, reefal carbonate deposition perturbations cause significant shifts in $\delta^{88/86}$Sr over the first 1-2 Myr of adjustment. After 5 Myr, the system re-equilibrates towards its initial values, reaching a near steady state at about 10 Myr. The transient isotope excursion results from the re-partitioning between reefal and pelagic carbonate deposition and affects $\delta^{88/86}$Sr and not ^{87}Sr/^{86}Sr. Using steady-state model simulations as a point of reference to interpret observed proxy changes would then lead to erroneous conclusions for the Sr system because there is no steady-state

change in seawater $\delta^{88/86}$Sr due to a step change in the neritic (reefal) $CaCO_3$ sink. (In contrast, ^{87}Sr/^{86}Sr is not affected by changes in the Sr sink associated with the neritic carbonate burial and thus does not vary at any point during this experiment.)

In Figure 3b, we present another example of how isotopic shifts can be time-dependent, in this example for the response to a CO_2 degassing change plotted in^{187}Os/^{188}Os versus δ^7Li space. Here, the mean ocean ^{187}Os/^{188}Os and δ^7Li isotopic compositions respond non-linearly in time because the equilibration timescales of the considered isotope systems and the C cycle each differ. With higher CO_2 outgassing, atmospheric CO_2 increases and climate warms, which then enhances continental weathering. This continues until higher CO_2 emissions are balanced by increased C loss through marine carbonate burial. The additional solute transfer from land to ocean under increased weathering shifts seawater ^{187}Os/^{188}Os to more radiogenic and continent-like values. This shift is not instantaneous but rather follows the progressive atmospheric CO_2 build-up towards the new equilibrium state on the silicate weathering timescale (>~10 kyr, Lord et al., 2016). Simultaneously, enhanced continental run-off initially drives seawater towards lower, more riverine δ^7Li. However, as dissolved Li accumulates in the ocean, Li is increasingly incorporated into marine secondary minerals. Since this process preferentially removes isotopically light Li, it counterbalances the isotopic effect of increased continental Li supply. Eventually, the preferential ^{6}Li burial drives seawater δ^7Li more positive, ultimately dictating the final steady-state ocean isotopic composition. Because enhanced sinks only compensate the effect of enhanced inputs of isotopically light continental Li supply after ~2 Myr, the δ^7Li shift reverses in sign.

These non-linear equilibrations of the $\delta^{88/86}$Sr, ^{187}Os/^{188}Os and δ^7Li systems illustrate how the isotopic fingerprint of a perturbation can fall far outside of a simple mixing line between two steady-state end members as the system adjusts to the perturbation. Consequently, the full range of isotopic shifts that could be recorded during the adjustment period can be much larger than the range of equilibrium states shown in Table 2 (illustrated in Figure SI.3)

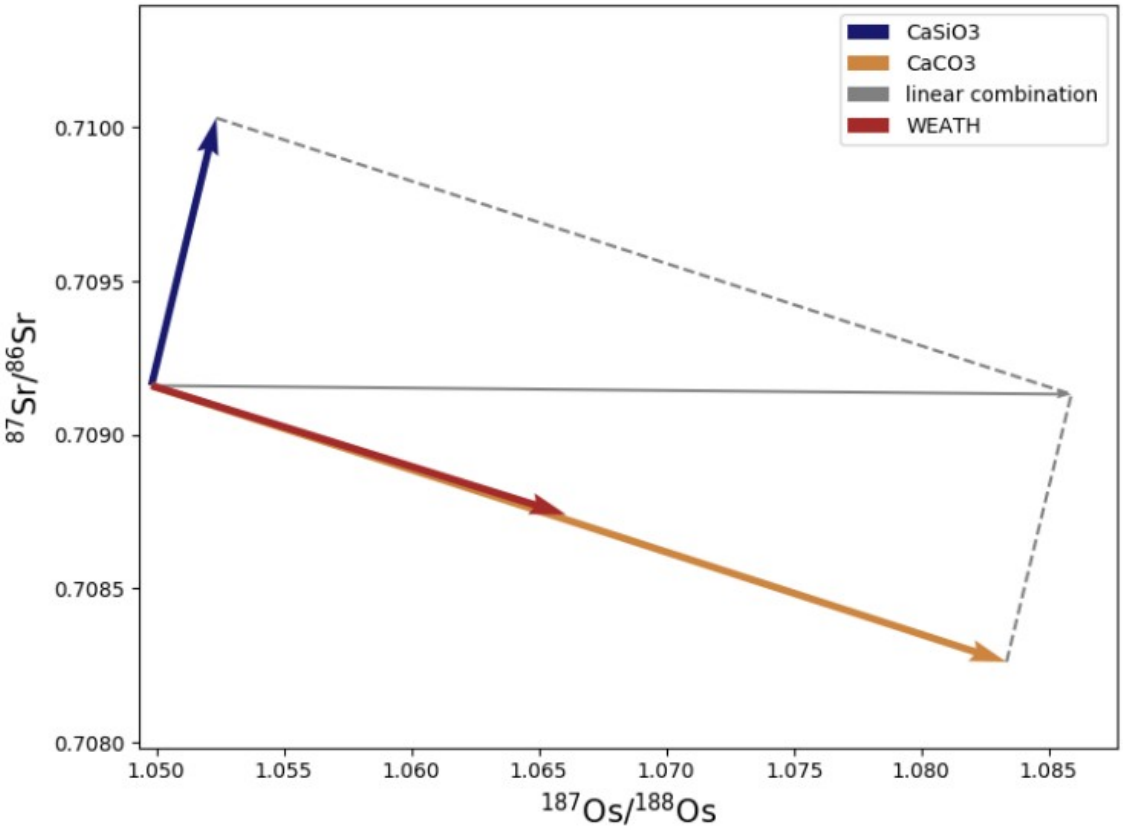

Figure 4: Evolution of $^{87}Sr/^{86}Sr$ and $^{187}Os/^{188}Os$ under doubled weathering fluxes in experiment series A. Shown are the isotopic effects of doubling $CaCO_3$ and $CaSiO_3$ weathering separately ('CaCO3' and 'CaSiO3' simulations) and at once ('WEATH' simulation). For comparison, the linear addition of the separate isotopic effects is indicated with gray lines.

We also find that changes in more than one boundary condition can cause additional non-linear effects on the isotopic composition of dissolved metals, further complicating the interpretation of isotopic signatures. For example, the combined impact on the Os/Sr isotopic systems of changing the weatherability of silicate and carbonate rocks does not equal the sum of their individual effects (Figure 4). In this example, the non-linearity results from the fact that changes in silicate weathering affect the climate, while, on the metal equilibration timescales, changes in carbonate weathering do not, and that silicate and carbonate rocks have different $^{87}Sr/^{86}Sr$. Doubling carbonate rock weathering proportionately increases the unradiogenic Sr and radiogenic Os supply to the ocean, shifting their isotopic ratios in the ocean in the corresponding directions. Conversely, increasing silicate weathering enhances CO_2 sequestration, reducing temperature. Eventually, the system reaches a new steady state, where silicate weathering balances the non-altered CO_2 outgassing once again. However, the steady-state climate is now cooler than before. This new cooler climate has a reduced carbonate weathering, tilting the ratio of silicate to carbonate weathering towards silicate weathering (source of radiogenic Sr), while keeping the total solute flux from land to the ocean almost constant, resulting in minimal changes in seawater $^{187}Os/^{188}Os$. However, when carbonate and silicate weatherability are increased simultaneously, the release of sedimentary Sr and Os is smaller than in the experiment with pure carbonate weathering

increase because of the cooling effect of more silicate weathering, yet it is larger than in the experiment with pure silicate weathering increase. Still, the final silicate-to-carbonate weathering ratio is tilted towards carbonate weathering when weathering of both lithologies are doubled simultaneously because the final colder climate reduces the carbonate weathering rate by less than half. Hence, when both lithologies are weathered more, seawater $^{87}Sr/^{86}Sr$ and $^{187}Os/^{188}Os$ shift in the same direction as if carbonate rock weathering alone was increased, but not to the same extent because of the increased silicate rock weathering cooling the climate.

3.2 Overprinting of solid Earth/ocean fingerprints by climate feedback

In our second ('B') experiment series, we explored the impacts of solid Earth/ocean perturbations on the metal isotopic system for transient (rather than persistent) perturbations, in particular the isotopic response to the temporary release of exogenic (mantle-like) C and/or metals into the atmosphere-ocean system. We analyse the simulations with a focus on disentangling the primary effects of exogenic metal fluxes and secondary effects of climate and C cycle feedbacks in the recorded isotope excursions.

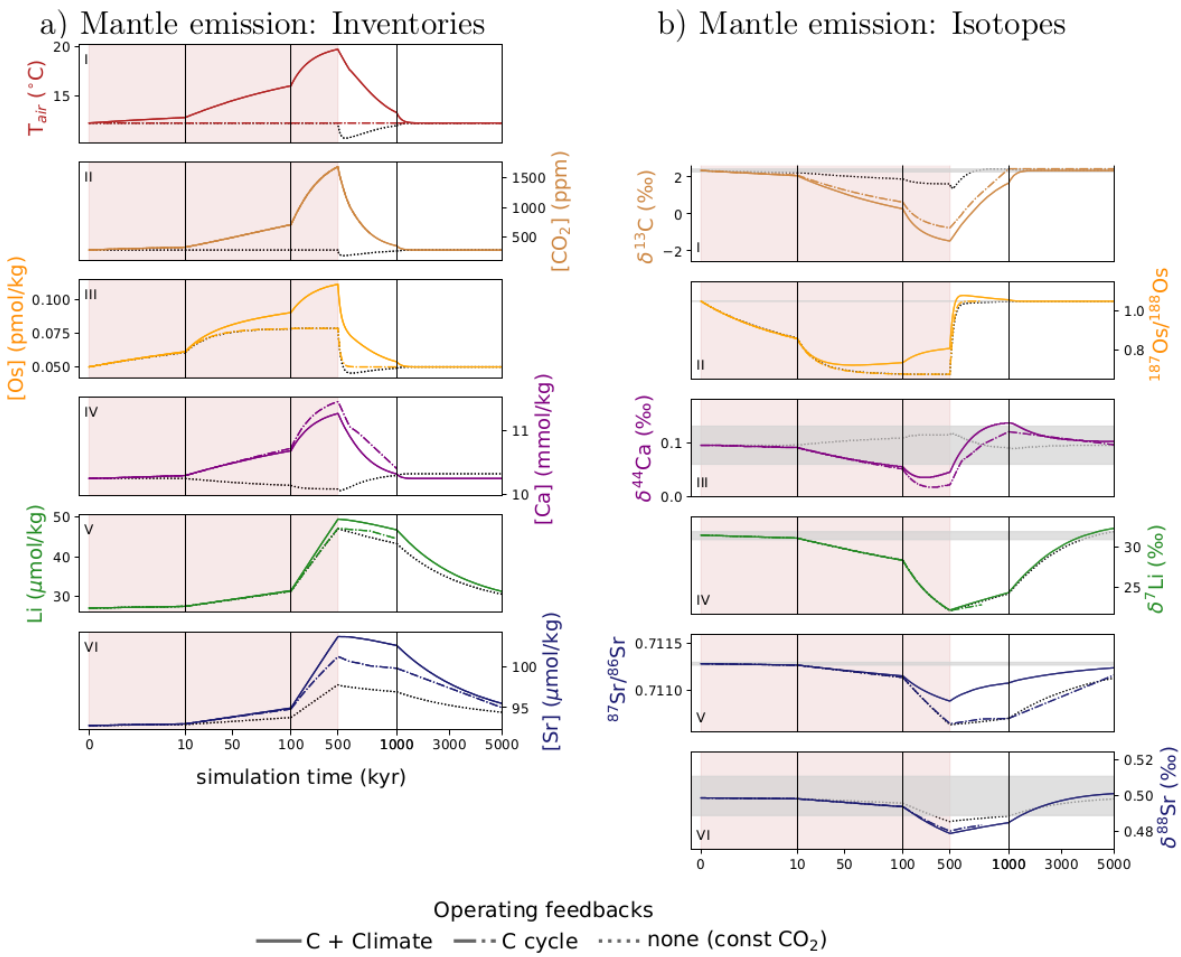

Figure 5: Competing transient isotopic effects in the response to extended emissions of carbon and metals from the mantle in experiment series B. a-b) Separation of contributions of exogenic ('no feedbacks', black dotted line), continental (difference between coloured 'C + Climate' and 'C cycle' lines) and sedimentary (difference between 'C cycle' and 'no feedbacks') metal injections to the simulated metal isotope excursions in the scenario

of 10x pre-industrial hydrothermal emissions, sustained over 500 kyr. Horizontal gray bands indicate intervals of assumed analytical uncertainty (see Methods).

To disentangle the role of C cycle feedbacks in the isotopic response to a large mantle emission, we ran a set of 3 experiments incorporating a continuous injection of mantle-derived metals over 500 kyr, running these (i) only with the enhanced trace-metal flux, (ii) with simultaneous C emissions but no climate feedback (i.e., an imposed invariant climate state), and (iii) all fluxes and including climate feedback (Figure 5). In the simulations with C emissions, atmospheric CO_2 concentrations increase throughout the duration of the emissions reaching maximum values at the point when emissions cease with a continuous relaxation afterwards. $\delta^{13}C$ and temperature values peak and relax back at a slower rate than CO_2 reflecting the log2 relationship between CO_2 and temperature and the C residence time in the ocean and atmosphere. We consider the responses of trace-metal inventories and isotopic composition separately in the sections that follow.

3.2.1 Trace metal inventory response

Among the metal systems, Os (Figure 5a III) is the fastest metal system to respond to the forcing due to its shorter residence time (~20 kyr in the pre-industrial ocean, compared to ~2 Myr for Sr, ~2.6 Myr for Li, ~1 Myr for Ca; Adloff et al., 2021). Regardless of whether or not climate feedbacks are included, Os concentrations peak at the end of the interval of enhanced emissions (model year 500,000) and then monotonically decline following two distinct recovery timescales: 1) the removal of excess marine Os that was injected from the mantle, on a time-scale dictated by its comparably short residence time (20 kyr) and 2) the decay of excess Os flux from weathering, on the time-scale of the silicate weathering-driven recovery of atmospheric pCO_2 and climate (ca. 200 kyr).

The simulated Ca reservoir remains largely invariant in the experiment without C addition, with only a small decline in concentration apparent over the 500 kyr duration of emissions. Because the enhanced metal flux is added at the seafloor in the model, deep ocean Ca concentrations become elevated relative to the ocean as a whole. carbonate preservation in deep sea sediments is enhanced, and the rate of loss of Ca from the ocean temporarily exceeds total input. Paradoxically, the increased flux of Ca at the seafloor leads to an overall reduction in the mean concentration of Ca in the ocean. At the end of the interval of enhanced input, carbonate preservation falls, driving the accumulation of Ca and alkalinity in the ocean and a corresponding drop in atmospheric pCO_2, and taking place on the ca. 10 kyr time-scale of carbonate compensation (Ridgwell and Hargreaves, 2007). In the experiment with C emissions (but no climate feedback), declining ocean carbonate saturation causes a reduction in the deep ocean carbonate sink and Ca rapidly builds up in the ocean over 500 kyr. Once the enhanced C flux ceases, the Ca inventory progressively adjusts back. Adding a climate response changes results in a somewhat reduced ocean Ca inventory response compared to this, with a smaller peak magnitude and a faster recovery driven by the ca. 200 kyr time-scale silicate weathering feedback.

The ocean concentrations of both Sr and Li peak at the end of the excess mantle metal input, as per the behaviours of the other metals as well as that of C. Following cessation of metal emissions and regardless of whether or not climate feedbacks are taken into account and/or there is coeval C release, the transient recovery response of the Sr and Li

reservoirs are dominated by their long inherent residence times in the ocean. However, for Sr, the magnitude of the inventory peak is enhanced when C is added to the system, with sediment dissolution and reduced carbonate preservation and burial enhancing the temporary accumulation of dissolved marine Sr. The oceanic Sr inventory response is enhanced still further when climate feedbacks are enabled. However, for the Li system which lacks a significant carbonate associated sink, the response to C forcing in the absence of climate feedbacks is almost indistinguishable from the response of metal emissions alone. Climate feedbacks drive an increased solute supply from land and accumulation of Li in the ocean. However, the impact of this is minor and there is relatively little separation between the three response curves for Li. This is because our model does not include a climate sensitivity of terrestrial clay formation (see: Adloff et al., 2021). We conducted a sensitivity experiment to test for the signal of changing weathering intensity, rather than rate, on the marine Li cycle, which is substantially larger (see discussion below and in the SI).

3.2.2 Trace metal isotope response

With the exception of Ca, mantle metal injection alone (dotted lines in Fig 5b) drives negative excursions in all isotope proxies, with the excursion nadir approximately coincident with the end of the excess emissions phase. The very minor positive $\delta^{44/40}$Ca is a consequence of the small but apparently paradoxical Ca inventory drawdown in response to enhanced mantle input (see previous discussion).

Coeval C addition (without climate feedback) has effectively no impact on ^{187}Os/^{188}Os, ^{87}Sr/^{86}Sr, or δ^{7}Li. As per for the response of the ocean Sr inventory, adding C and acidifying the ocean (and reducing saturation state) suppresses the carbonate-hosted sinks of Sr and drives a more negative excursion in $\delta^{88/86}$Sr. δ^{13}C is directly impacted by the addition of isotopically light C and undergoes a substantial almost -4‰ excursion. In contrast, without C injection, only a minor negative fluctuation of δ^{13}C occurred due to a repartitioning of C between ocean and atmosphere and changes in carbonate burial induced by Ca injection. $\delta^{44/40}$Ca exhibits the greatest impact as a consequence of ocean acidification and what was a very muted positive isotopic excursion now becomes larger in magnitude and negative, with its nadir aligning with the end of emissions as per the other isotope systems.

Climate changes and enhanced weathering induced by C release notably reduce the excursion amplitude of the radiogenic isotope systems (^{187}Os/^{188}Os, ^{87}Sr/^{86}Sr) while having little effect on stable isotope proxies. This difference is primarily a consequence of how enhanced weathering amplifies the metal inventory excursion magnitude for Os and Sr concentrations (Fig 5a and previous discussion) as compared to e.g. Li for which the climate feedback has only a negligible impact, and Ca where climate feedback slightly ameliorates the inventory response. Marine $\delta^{44/40}$Ca is only meaningfully perturbed by C cycle changes, with and without climate feedbacks, as a consequence of changes in the marine carbonate sink induced by C addition to the ocean (and atmosphere). δ^{7}Li is the only proxy which is virtually insensitive to our simulated C cycle perturbation because of the static δ^{7}Li in continental run-off in these simulations (see discussion below and in the SI).

Without climate feedbacks included (or no C release at all, with the exception of $\delta^{44/40}$Ca), all isotope systems reach their excursion nadir approximately coincident with the end of the excess emissions phase. However, accounting for feedbacks can dramatically impact the relative timing or duration of an isotopic excursion, most notably for ^{187}Os/^{188}Os and ^{87}Sr/^{86}Sr, but also for $\delta^{44/40}$Ca and δ^{13}C. For instance, we find that the nadir of the ^{187}Os/^{188}Os excursion peak occurs 10s of kyr earlier if feedbacks operate. For ^{87}Sr/^{86}Sr, climate feedback enables a much more rapid initial (first 500 kyr following the end of enhanced emissions) recovery in the isotopic composition of the ocean and hence a sharper excursion as compared to the simulation without feedbacks. Furthermore, depending on the relative scale of the C cycle perturbation (see: SI), isotopic excursions caused by igneous metal supply can be masked in some isotope systems. Examples are the minor positive $\delta^{44/40}$Ca excursions in simulations without C emissions and the strongly dampened negative ^{87}Sr/^{86}Sr excursion in simulations with strong C forcing (simulation 2xC:Metal$_{HYD,}$ see figures SI.5 and SI.6).

With the exception of C, the recovery phase in all the isotope systems are characterized by the occurrence of a positive isotopic excursion. The timing of the positive excursion following termination of mantle input generally scales with metal residence time – shortest for Os, and longest for Sr and Li (and in fact only partially resolved without the 5 Ma total model experiment duration for these systems). This occurs as a consequence of the rate of metal burial, driven by enhanced metal inventories, exceeding metal supply (as the prescribed mantle flux ceases and enhanced fluxes from weathering decline). This leads to a temporary accumulation of the heavier isotopes in seawater due to burial-associated fractionation which is recorded as a positive excursion.

In general, the different isotopic responses to emissions stem from feedbacks within the global C cycle and with climate – primarily continental weathering changes. The role of continental weathering in modulating the marine Os, Sr, Li and Ca reservoirs, shown as part of experiment series A, have long been recognized and inspired the use of these isotope systems to trace changes in continental weathering (e.g., Gannoun et al. 2006, Blättler et al. 2011, Lechler et al. 2015). Higher atmospheric CO_2 concentrations and a warmer and wetter climate enhances weathering which then adds more continental-derived metals to the ocean, shifting ocean values towards continental-like values. Yet, our experiment series B shows that this effect can compete with the isotopic effect of metal emissions from the mantle and reduce both ^{187}Os/^{188}Os and ^{87}Sr/^{86}Sr excursion amplitudes if an igneous event spans weathering-relevant timescales. We also notice that if the C forcing is sufficiently strong and long-lasting, enhanced continental weathering leads to the partial recovery of the initial negative Os and Sr isotopic excursion despite continued mantle emissions (see: SI). Even when mantle emissions cease, enhanced continental weathering prevails because temperature is still elevated, driving the seawater composition back to pre-event values more quickly than without climate-driven weathering increases. In extreme cases, enhanced weathering accelerates the ^{187}Os/^{188}Os and ^{87}Sr/^{86}Sr recoveries so much that it can lead to positive 'overshoot' excursions after the emissions event (Figure SI.5b).

For stable metal isotopes, C cycle-induced isotopic forcings are more subtle. Increased input from weathering does not constitute an opposing isotopic forcing to igneous input as in the case of radiogenic isotopes. Due to isotopic fractionation during burial, the

steady state marine reservoirs of Sr, Li and Ca are inherently relatively more heavy than in hydrothermal and continental inputs. Therefore, enhanced continental weathering amplify the tendency towards isotopically lighter stable Sr, Li and Ca in seawater caused by mantle inputs, rather than counteract it. Additionally, stable metal isotope ratios depend on the sedimentary burial flux which is also sensitive to C cycle-driven changes. Since marine carbonate burial controls seawater $\delta^{88/86}$Sr and $\delta^{44/40}$Ca, changes in carbonate burial due to C emissions create additional isotopic forcings, even if it only effects the marine carbonate system and the climate remains unchanged. C injections transiently reduce the carbonate saturation state in the ocean, and thus the chemical stability of sedimentary Ca carbonate, while the climate-driven additional growth of the marine Sr, Ca, and Li reservoirs enhances stable isotope fractionation during carbonate burial. In the case of $\delta^{88/86}$Sr, C emissions increase the amplitude of the negative excursion caused by the mantle input of isotopically lighter Sr due to acidification-driven reductions in net carbonate burial (from more dissolution), retaining and releasing more of the preferentially buried ^{86}Sr into the ocean. For $\delta^{44/40}$Ca, increased hydrothermal Ca input alone is insufficient to cause an isotopic shift because the marine Ca reservoir is dominated by rock and sediment dissolution and formation (see continental/hydrothermal influx ratio in Table SI.4). Similarly, enhanced continental Ca input is also insufficient to induce a measurable excursion over the tested emissions duration because of the large size of the marine Ca reservoir. Our model simulations instead suggest that marine carbonate formation and dissolution are the dominant controls on seawater $\delta^{44/40}$Ca. In response to a C release event, marine carbonate burial is first reduced by seawater acidification and then subsequently increased by additional continental and sedimentary alkalinity supply, causing a negative followed by a positive $\delta^{44/40}$Ca excursion. Enhanced continental weathering thus affects the $\delta^{44/40}$Ca excursion predominantly more via marine carbonate buffering than directly adding isotopically light Ca. The effects on the marine Li reservoir are different than for Os, Sr, and Ca in these simulations, because the isotopic composition of continental weathering is much closer to the initial seawater δ^{7}Li value than is hydrothermal input. Furthermore, with a 10-fold increase in hydrothermal and C emissions, weathering only quadruples. Thus, the hydrothermal forcing dominates the negative δ^{7}Li excursions in our simulations with climate and C cycle dynamics playing only a minor role in changing supply fluxes. It should be noted that this dominance only exists when the isotopic composition of riverine Li remains constant (as assumed in these simulations). When we varied the isotopic composition of Li in terrestrial run-off according to expected shifts with increasing weathering intensity, we found that they can cause a similar marine δ^{7}Li perturbation as the most extreme simulated hydrothermal emissions (see Li case study in the SI).

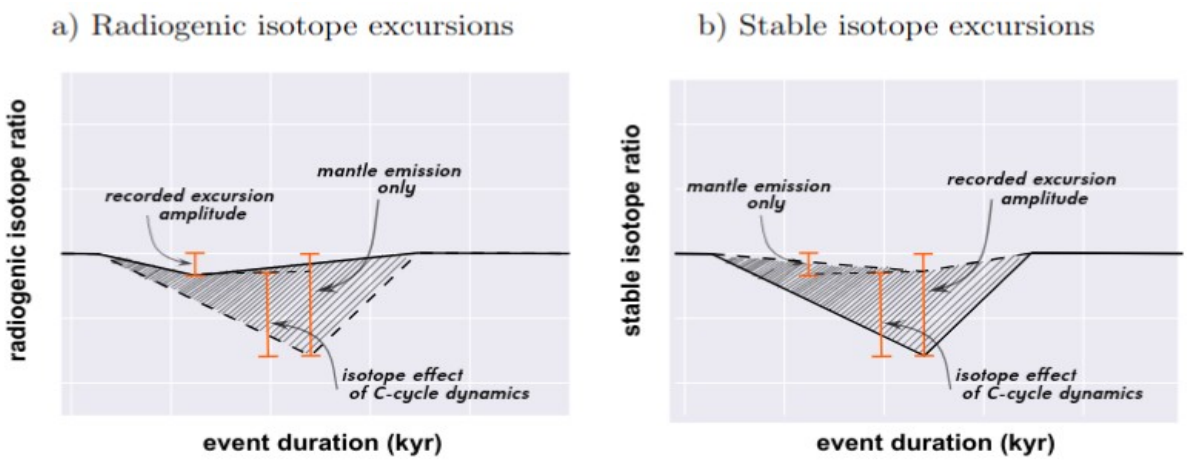

Figure 6: Conceptualization of contributions of mantle emissions and C-cycle dynamics to the recorded excursion amplitudes in radiogenic (e.g. $^{187}Os/^{188}Os$ and $^{87}Sr/^{86}Sr$) and stable (e.g. $\delta^{88}Sr$, $\delta^{7}Li$, $\delta^{44}Ca$) isotope proxy systems.

Our experiments show how C inputs, and associated changes in seawater chemistry as well as global climate and continental weathering, affect the shape and size of metal isotope excursions. Recorded metal isotope excursions following igneous events hence contain quantitative information about both the primary metal release to the ocean, and the sediment dissolution and climate-related weathering responses. However, a challenge remains in disentangling the forcing from the feedback signals. Our simulations suggest that the amplitudes of radiogenic Os and Sr excursions are insufficient to constrain perturbations of continental or mantle metal supply because C cycle feedbacks potentially reduced the size of unradiogenic $^{187}Os/^{188}Os$ and $^{87}Sr/^{86}Sr$ excursions during mantle emission events. In particular, if the response timescale of a proxy is similar to, or exceeds, the C cycle feedback timescale, like for $^{87}Sr/^{86}Sr$ and continental weathering (~200 kyr, Lord et al., 2016), the underlying exogenic forcing can be masked almost entirely. For instance, if we were to estimate the magnitude of mantle emissions directly from the size of a recorded $^{87}Sr/^{86}Sr$ excursion, we would underestimate it by up to 85% if terrestrial weathering were perturbed (Figure SI.7). However, with an independent estimate of the Sr input from the mantle (i.e., using the volume and composition of a large igneous province), we could quantify the scale of terrestrial Sr supply changes by comparing the recorded isotope excursion and the expected excursion from the mantle input only. This is conceptualised in figure 6. For the radiogenic isotopes ($^{187}Os/^{188}Os$ and $^{87}Sr/^{86}Sr$), the recorded isotopic excursion equals the portion of the exogenic forcing that was not compensated for by enhanced terrestrial metal delivery. On the other hand, the recorded excursion of stable isotope systems ($\delta^{88/86}Sr$, $\delta^{7}Li$, $\delta^{44/40}Ca$, Figure 6b) represents the sum in isotopic forcings, which deliver metals from the land, the mantle and carbonate burial.

4. Discussion

Records of the isotopic composition of sedimentary C, Sr, Os, Li and Ca have been widely used to infer changes in the solid Earth-ocean interactions, both on tectonic timescales (e.g. Misra and Froehlich 2012, Mills et al., 2014, Mills et al., 2017) and for geologically rapid perturbation events (e.g. Jones and Jenkyns, 2001, Tejada et al., 2009, Blättler et al., 2011, Lechler et al., 2015). Our experiments provide new insights into the timescale and persistence of isotopic shifts in response to such changes in a fully coupled Earth system.

4.1. Identifying long-term shifts in the coupling of Earth's surface reservoirs and geosphere

Our experiments show how fingerprints of the processes underlying shifts in solid Earth-ocean interactions can be identified by combining records of multiple metal isotope systems and C cycle proxies – something that is not possible with individual isotope records alone. Additionally, our results highlight the different ways in which the C cycle (and climate feedbacks) affects metal cycles and the necessity to interrogate metal and C cycle changes together within a common framework. We showed, for example, that the dominant long-term effect of increased exposure of silicate rock to weathering under constant CO_2 degassing is not a higher flux of silicate-derived metals to the ocean but a reduced metal supply from non-silicate rocks due to a colder new steady-state climate with similar silicate weathering rates (Table 2 and Figure 4). The fingerprints of step changes in solid Earth-ocean interactions can be identified most clearly in a new steady-state of metal and C cycles. In this case, Figure 2 and Table 2 showed which Earth system changes can cause isotopic shifts of a given direction and magnitude. However, prior to a new steady state being reached, the amplitude and direction of the isotopic shifts in different proxy systems – absolute and relative to each other – may vary non-linearly over time and outside the envelope of the two bounding steady-states, as the system adjusts to the new conditions. Given the long equilibration time of the Sr, Li and Ca cycles, it is questionable whether they have ever reached true equilibrium at any point during the Phanerozoic in face of continuous tectonic movement and changes in climate. Therefore, transient, non-linear features of the equilibration process, differences in equilibration timescales of different biogeochemical cycles, and the possibility of overlapping Earth system changes, also need to be considered in the interpretation of the Phanerozoic record of metal and C isotopes. We showed that simulating coupled metal and C cycles provides a useful tool to explore non-linear combinations of isotopic forcings from several simultaneous Earth system changes and transient features of the equilibration which can obscure the cause of long-term isotopic shifts and may also result in decoupling of the different systems.

Our findings provide a systematic numeric basis for interpretations of long-term Os, Sr, Ca and Li isotope variations in the geologic record. For example, during the Cenozoic, the Earth system markedly changed from the hot-house climate of the Early Cenozoic to the ice-house climate of the Quaternary, which has been linked to changes in C cycling between the solid Earth and the ocean/atmosphere. From the isotopic differences in sedimentary Os, Sr, Ca and Li, it has been suggested that the transition from hot- to ice-house climate resulted

from changes in weathering and/or erosion due to orographic events or climate and hydrothermal changes (e.g. Raymo et al., 1988, Richter 1992, Goddéris and Francois, 1995, Pegram et al., 1992, Li et al, 2007, Misra and Froelich, 2012). In our simulations, weathering or hydrothermal changes were insufficient to produce all of the isotopic shifts required to explain the Cenozoic record. The only process we could identify to be strong enough to produce such large shifts (in the isotopic composition and not necessarily in the rate) is a compositional change in terrigenous dissolved metal input, i.e. the weathering of much younger rocks that can transfer ions efficiently into the open ocean at the beginning of the Cenozoic. While we would need to test this scenario with boundary conditions specific to the Early Cenozoic for a more conclusive quantitative analysis, our results suggest that the long-term isotopic changes across the Cenozoic are likely a complex, non-linear result of combined forcings. The Cenozoic record also contains evidence of transient isotopic shifts. For example, Paytan et al. (2020) used records of stable and radiogenic Sr isotope changes to identify transient changes in the mass balance of dissolved Sr. They concluded that $\delta^{88/86}$Sr shifts in the Cenozoic record reflect most likely transient imbalances in the Sr budget, i.e. through increased removal due to shelf expansion. Our simulations confirm that $\delta^{88/86}$Sr excursions can only be a transient feature of Sr cycle changes, though they can persist for several million years depending on the scale of the Sr flux imbalance.

4.2 Lessons for the reconstruction of metal fluxes from recorded isotope excursions

C, Sr, Os, Li and Ca isotopes are also used to investigate perturbations on shorter timescales (e.g. LIP volcanism and bolide impacts). For example, these proxy systems have been used to identify and quantify excess igneous and continental C and metal fluxes during OAE 1a and 2, the Deccan Traps and the Chicxulub impact and the PETM C excursion discussed in the introduction (e.g. Jones et al., 2001, Ravizza et al., 2001, Blättler et al., 2011, Lechler et al., 2015, Pogge von Strandmann et al., 2013, Bauer et al., 2017). Some of these events were predominantly characterized by increased metal emissions from the mantle or impact ejecta, while others also featured alterations of metal fluxes from sediments and the continental crust via perturbations of the C cycle. Although our model experiments are idealized, the applied metal and C injections share many characteristics with these real geologic events. Simulations of pure C emissions may represent any change in continental weathering regime that is not accompanied by metal emissions from the mantle, i.e. activation of dormant superficial C reservoirs (e.g. methane emissions from peatlands, permafrost or hydrates, expansion or shrinking of the biosphere etc.) or changes to rock exposure, e.g. through variations in the extent of glacial land cover, sea-level fluctuations or similar. Simulations of pure exogenic emissions may represent bolide impacts, provided that the impact did not significantly perturb superficial C reservoirs, although C-neutral impacts of asteroids sufficiently large to provide enough metals to disturb the marine reservoirs of Os or Sr are arguably unlikely (Kamber et al. 2019). Our coupled metal and C emission experiments micmic LIP emplacements, during which isotope systems were shaped simultaneously by magmatic and continental inputs, since they were characterized by sustained, large-scale outpourings of magma with mantle-like isotopic composition and super-saturated in CO_2 which caused climatic shifts upon release (e.g. Ernst 2014). The results of our experiments can also be used to estimate the isotopic effect of emissions with different Sr:Os:Li:Ca ratios by combining results of simulations with different emission rates (e.g. taking Os results from a simulated doubling of hydrothermal emissions and Ca results from a simulated

quadrupling) to study cases where the ratios between emitted metals were different to today's hydrothermal systems assumed here - because the metal cycles do not interact with each other.

Our simulations showed that C emissions affect the shape of resulting metal isotope excursions during metal release from the mantle: Injection of C alongside mantle-derived metals increases the amplitudes of negative and positive stable isotope excursions. At the same time, it decreases negative excursions in radiogenic isotope systems and can cause positive overshoots. C emissions also change the timing of the negative $^{187}Os/^{188}Os$, $^{87}Sr/^{86}Sr$ and $\delta^{44/40}Ca$ excursion peaks: These excursion peaks co-occur at the end of metal emissions in simulations without excess C emissions (see also figure SI.8). When mantle-derived metal inputs are accompanied by C emissions, the excursion peaks are temporally offset because metal fluxes from land and sediments are also perturbed and influence marine isotopes, in addition to the mantle emissions. Marine metal reservoirs grow substantially larger in simulations with excess metal and C emissions because of metal supply from the mantle and climate-driven solute influxes from land. The isotopic impacts of perturbed metal fluxes from the mantle and lithosphere likely overlap temporally and need to be disentangled in order to separate the magnitude of the forcing from any weathering feedbacks.

Thus, if radiogenic isotope excursions during C cycle perturbations were interpreted as purely mantle emission-driven, the igneous forcing would be underestimated because radiogenic isotope systems are also affected by continental input changes. Similarly, the interpretation of stable isotope excursions during a C cycle perturbation as pure weathering signals would overestimate the scale of weathering changes, mainly since disruption to carbonate burial is a relevant driver of $\delta^{88/86}Sr$ and $\delta^{44/40}Ca$ excursions. The extent of this under- or overestimation depends on the ratio of emitted C to metal released from the mantle and the background state (see discussion in section 4.3). Still, radiogenic and stable isotope excursions can provide end-member estimates of excess igneous, continental inputs and carbonate burial changes because each proxy system has different sensitivities to the perturbed fluxes. Additional and independent constraints are required to increase the accuracy of these metal and C flux estimates (e.g. reconstructed C:Metal of igneous emissions, metal and C mass constraints from estimates of amount and composition of the emplaced basalt or independent evidence on the strength of climate feedbacks). These findings show that the geochemical record of igneous events can be more complex than the coincidence of a negative $\delta^{13}C$ and mantle- or continent-like metal isotope excursions. Dynamic models of combined C and metal cycling are required to reconstruct the total exogenic forcing.

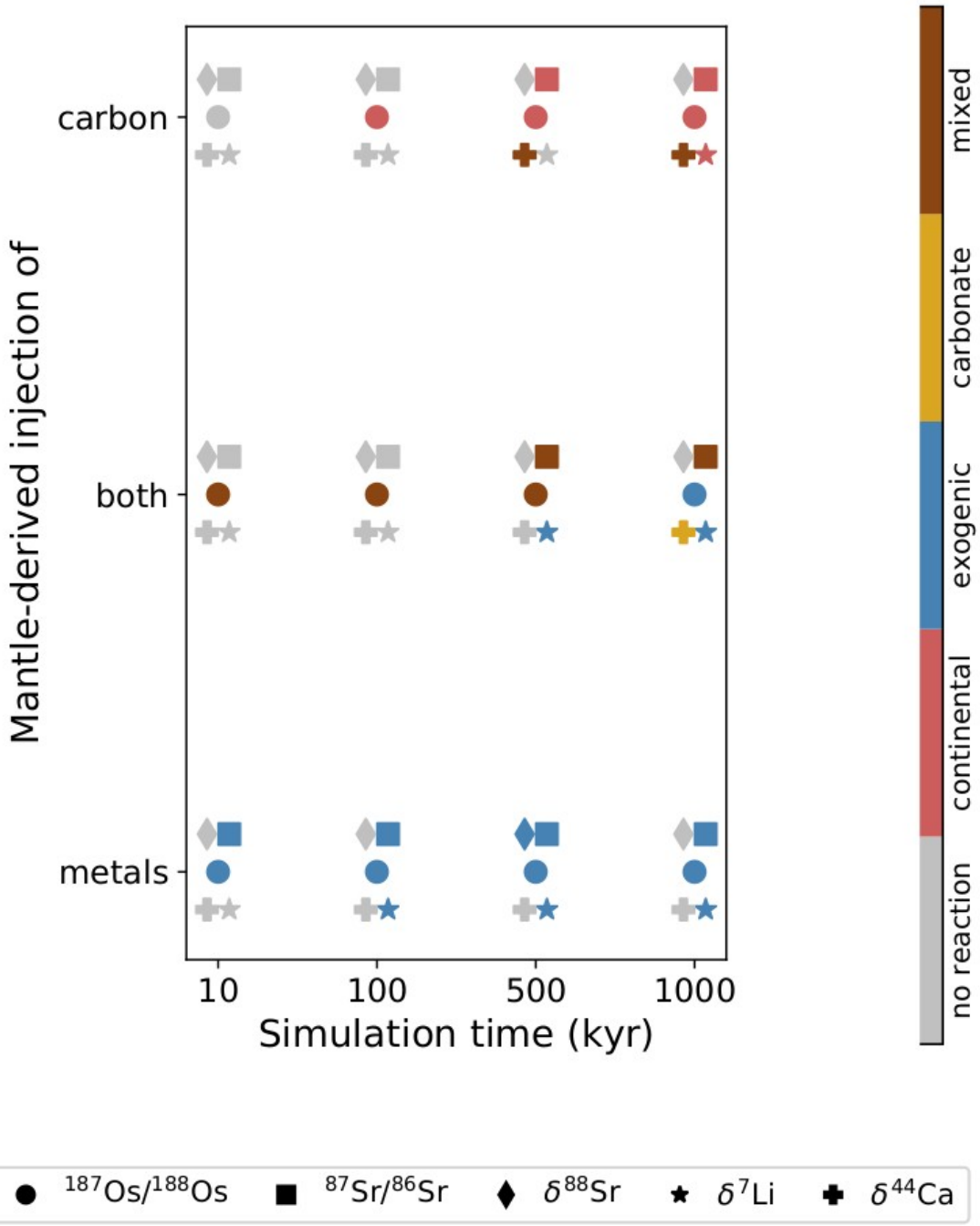

Figure 7: 'Proxy potential' of seawater $^{187}Os/^{188}Os$, $^{87}Sr/^{86}Sr$, $\delta^{88}Sr$, $\delta^{7}Li$, $\delta^{44}Ca$ changes across a simulated 500 kyr long hydrothermal event in ensemble B with ten-fold pre-industrial hydrothermal metal release and varying amounts of C emissions. Each proxy system is represented by a different marker shape. Colours indicate if a measurable (considering a theoretical analytic error) isotopic excursion at the given time into the event is directly attributable to exogenic (mantle-derived) metal emissions, continental input due to enhanced weathering, carbonate dissolution or whether more than one of these processes shape the excursion. The assumed analytical uncertainties are: 0.02 ($^{187}Os/^{188}Os$), 0.0001 ($^{87}Sr/^{86}Sr$), 0.01‰, ($\delta^{88}Sr$), 0.1‰, ($\delta^{7}Li$) and 0.05‰, ($\delta^{44}Ca$).

We can translate the results of our idealized simulated metal emissions events into useful information to quantify the relative contributions of mantle-derived metal emissions, enhanced continental crust weathering, and reduced carbonate burial to metal isotope excursions, and thus to estimate the dominant control on each metal isotope proxy in different

circumstances. As an example, we identify the metal source that dominates the isotopic response of each proxy system at different time points in the simulation as a result of a large mantle emission event, e.g. during ocean plateau emplacement (Figure 7 and SI.9). We found that several proxy systems only show isotope excursions outside of analytical uncertainty (Table SI.3) after substantial cumulative excess metal input, either due to a sufficiently long event duration or high emissions rates, because of the long marine residence times. Notably, none of our simulations resulted in a $\delta^{88/86}$Sr excursion outside of analytical uncertainty, corroborating previous findings that it is a better proxy for lasting changes in Sr removal (and carbonate formation) than transient perturbations of Sr inputs (Paytan et al., 2021). ^{187}Os/^{188}Os and ^{87}Sr/^{86}Sr have variably been used as identifiers of enhanced weathering fluxes or volcanic episodes. Our results in Figures 5 and 6 show that these interpretations work best when only one input flux is perturbed. If Os and Sr input from weathering and Earth's interior are altered simultaneously, the resulting isotopic excursion integrates both effects. $\delta^{44/40}$Ca is predominantly an indicator of carbonate rock weathering increases or sediment dissolution in response to sustained C injection. The weak response of δ^{7}Li to weathering changes in our experiments reflects the fact that this proxy is mostly sensitive to changes in weathering congruency rather than the size of the weathering flux (e.g. Pogge von Strandmann et al., 2020).

4.3 Model limitations and the importance of background state

The applicability of the numeric results of this study to past events is limited by the dynamic processes contained in the model. Most importantly, in our simulations, climate change only affects weathering fluxes in the global mean, with globally averaged weathering fluxes scaled to temperature and precipitation (Colbourn et al., 2013). Our simulations did not account for spatial variations in weathering rate, erosion, or exposure due to climate change. Such variations could affect solute fluxes to the ocean and their isotopic composition, as both climate change over land and terrestrial geology are spatially very heterogeneous (e.g. McCabe et al., 2013, Bayon et al., 2021). Similarly, our simulations did not consider temporal variations in solute or isotope fluxes due to maturing of weathered surfaces (e.g. Miller et al., 2015).

The applicability of our results to past events is further limited by the assumed background Earth system and initial states of C and metal cycles, since we based our simulations on a present-day configuration of continents, climate, and biogeochemical cycling. In several ways, the background state influences the impacts of transient or lasting changes in solid-Earth ocean interactions on marine metal reservoirs and their alteration through the C cycle. One uncertainty arises from the isotopic offset between metal reservoirs as it dictates how much a metal transfer from one reservoir to the other affects their isotopic composition. For example, continental input changes have smaller isotopic effects if the seawater signature is already close to the continental end member. Isotopic fractionation factors also need to be considered when interpreting isotopic shifts in the geological record. Our simulations produced smaller $\delta^{88/86}$Sr and $\delta^{44/40}$Ca fluctuations than reconstructed for past events (e.g. Fantle and Ridgwell, 2020, Paytan et al., 2021), which may highlight the importance of fractionation factor changes, authigenic carbonate precipitation or diagenesis in real-world events that were not captured by our simulations.

For transient events, the pre-event ratio of continental versus mantle-derived inputs dictates the sensitivity of a marine metal reservoir to C cycle changes. The modern-day ratio is lowest for Li and largest for Ca, indicating the smallest and biggest sensitivities to enhanced weathering, respectively. Os and Sr have the same ratio of modern-day continental versus mantle-derived inputs. Yet, the simulated behavior of $^{187}Os/^{188}Os$ and $^{87}Sr/^{86}Sr$ under igneous forcing and the impacts of C cycle changes is different because of the vastly different initial marine reservoir sizes and residence times. Os has the smallest initial ocean inventory and residence time of the studied metals. Hence, its marine reservoir shows measurable perturbations more quickly than those of other metals. In simulations of simultaneous mantle-derived metal and C emissions, most of the $^{187}Os/^{188}Os$ excursion builds up before the isotopic forcing of climate-driven increases in continental crust weathering manifests. Isotopic effects of igneous metal emissions and C cycle changes are almost temporally separate in the resulting $^{187}Os/^{188}Os$ record. At the same time, they overlap, and in some simulations, cancel each other in the $^{87}Sr/^{86}Sr$ record because of the larger initial marine Sr reservoir and residence time. The strengths of continental and igneous isotopic forcings depend on the isotopic offset between metals in the mantle and continental run-off and seawater. For $\delta^{88/86}Sr$, $\delta^{7}Li$ and $\delta^{44/40}Ca$, the initial role of the marine sink for the isotopic composition of seawater is an essential control on the isotopic signal of the recovery of increased marine metal reservoirs. Furthermore, the climate sensitivity of C cycle feedbacks affects the strength and speed of the C cycle perturbation, which then manifests in metal isotope records.

A final aspect to consider is the initial size of a particular marine metal reservoir in the past (and how this may change through geological time) as it affects the inertia of the marine proxies. There are few constraints on the evolution of marine metal and C reservoir sizes through time. In this situation, studies commonly revert to assuming that the marine reservoir did not vary significantly over time and that isotopic changes in past seawater can be interpreted as if they happened in the modern ocean (e.g. Blättler et al. 2011, Bauer et al. 2017). Where metal reservoir variations have been considered, these assumptions were usually made independently of C flux changes (e.g. Blättler et al. 2011, Lechler et al. 2015) because of missing constraints on the processes that caused these variations. The range of process changes explored in our first (A) series of simulations lead to marine metal reservoirs that differ from the modern by up to 175% for Ca and Sr, 280% for Os, and 300% for Li. Changing one process can affect different metal systems differently, sometimes resulting in substantial differences in the relative reservoir size change that is induced. Sensitivity studies for the initial reservoir size, in addition to other poorly constrained boundary conditions (e.g. Kalderon-Asael et al., 2021), are important to estimate the uncertainty of quantitative interpretations of metal isotope records. The degree to which the background state can be constrained for past periods determines the uncertainties associated with the quantitative interpretation of metal isotope excursions.

Conclusion

In this study, we used an isotope-enabled, intermediate complexity Earth system model to examine the response of Os, Sr, Li and Ca isotopes and the C cycle to geological perturbations. The simulations show that isolated C, Ca, Sr, Os and Li isotope records are ambiguous indicators of flux changes between the geosphere and Earth's surface reservoirs because they respond to various geologic forcings. However, when combined and supported by independent proxies of C cycle changes, Ca, Sr, Os and Li isotopes provide unique fingerprints constraining the direction and magnitude of solid Earth-ocean exchange processes. Yet, detecting these fingerprints in the geologic record is complicated by the non-linearity of combined isotopic effects of multiple perturbations, differences in the reaction time of different proxy systems, and uncertainties about baseline elemental fluxes before the perturbation. These non-linearities and dependencies on background conditions could be explored and characterized in future work with coupled C and metal cycle simulations like the ones that we presented.

We also studied the isotopic effect of transient C and metal release events. We showed that all four proxy systems are sensitive to the isotopic forcings of enhanced igneous and continental metal emissions, and $\delta^{88/86}$Sr and $\delta^{44/40}$Ca also to changing carbonate burial rates. Since igneous inputs and C cycle changes both affect the record isotopic excursions, they need to be disentangled before the excursion amplitude can be used to constrain the size of excess metal and C fluxes during a perturbation event. We suggest combining the analysis of radiogenic and stable isotope systems is a practical first-order approach since they provide opposite end-member constraints on metal inputs from the mantle. More precise estimates of metal and C emissions based on isotope excursion amplitudes require assumptions about the background Earth system state (metal and C cycles). Uncertainties introduced by these unknown parameters can again be explored by Earth system model simulations considering links between the cycling of metals and C. Such simulations can also help estimate the time lags between excursion peaks in different isotope systems, which need to be known to correlate any given event across other metal and C cycle proxy records. A holistic view of metal and C dynamics will be essential for advancing our interpretations of past metal isotope excursions, on tectonic time scales and during shorter geologic events.

Acknowledgments

We thank Ian Parkinson, Philip Pogge von Strandmann, Alex Dickson and Dan Lunt for stimulating and informative discussions of our simulations. This work is a result of the NERC GW4+ Doctoral Scholarship for Markus Adloff (NE/L002434/1). NERC also provided funding for Sarah Greene (NE/L011050/1 and NE/P01903X/1) and Fanny Monteiro (NE/N011112/1 and NE/V01823X/1). A.R. acknowledges support from NSF grant EAR-2121165, as well as from the Heising-Simons Foundation.

Code availability

The code for the version of the ‘muffin’ release of the cGENIE Earth system model used in this paper, is tagged as v0.9.36 and is assigned a DOI: https://doi.org/10.5281/zenodo.7542440.

The specific branch of the code used for this paper was: `_DEV_FeNIP2`. Configuration files for the specific experiments presented in the paper can be found in the directory: genie-userconfigs/PUBS/submitted/Adloff_et_al.G3.2023. Details of the experiments, plus the command line needed to run each one, are given in the readme.txt file in that directory. All other configuration files and boundary conditions are provided as part of the code release. A manual (v0.9.33) detailing code installation, basic model configuration, tutorials covering various aspects of model configuration, experimental design, and output, plus the processing of results is available at github.com/derpycode/muffindoc/ (https://doi.org/10.5281/zenodo.7258577).

References

Adloff, M., Ridgwell, A., Monteiro, F. M., Parkinson, I. J., Dickson, A. J., Pogge von Strandmann, P. A., ... & Greene, S. E. (2021). Inclusion of a suite of weathering tracers in the cGENIE Earth system model–muffin release v. 0.9. 23. *Geoscientific Model Development*, *14*(7), 4187-4223.

Adloff, M., Greene, S. E., Parkinson, I. J., Naafs, B. D. A., Preston, W., Ridgwell, A., ... & Monteiro, F. M. (2020). Unravelling the sources of C emissions at the onset of Oceanic Anoxic Event (OAE) 1a. *Earth and Planetary Science Letters*, *530*, 115947.

Alt, J. C. and Teagle, D. A. (1999). The uptake of C during alteration of ocean crust. Geochimica et Cosmochimica Acta, 63(10):1527–1535.

Bain, D. C., & Bacon, J. R. (1994). Strontium isotopes as indicators of mineral weathering in catchments. *carbonatena*, *22*(3), 201-214.

Banerjee, N. R. and Muehlenbachs, K. (2003). Tuff life: bioalteration in volcaniclastic rocks from the Ontong Java Plateau. Geochemistry, Geophysics, Geosystems, 4(4).

Bauer, K. W., Zeebe, R. E., & Wortmann, U. G. (2017). Quantifying the volcanic emissions which triggered Oceanic Anoxic Event 1a and their effect on ocean acidification.*Sedimentology*, *64*(1), 204-214.

Bayon, G., Freslon, N., Germain, Y., Bindeman, I.N., Trinquier, A. and Barrat, J.A., 2021. A global survey of radiogenic strontium isotopes in river sediments. *Chemical Geology*, *559*, p.119958.

Berger, W., Smetacek, V., and Wefer, G. (1989). Ocean productivity and paleoproductivity—an overview. In Productivity of the ocean: present and past, volume 44, pages 1–34. Wiley New York.

Black, B. A. and Gibson, S. A. (2019). Deep C and the life cycle of large igneous provinces. Elements: An International Magazine of Mineralogy, Geochemistry, and Petrology, 15(5):319–324.

Blättler, C. L., Jenkyns, H. C., Reynard, L. M., and Henderson, G. M. (2011). Significant increases in global weathering during Oceanic Anoxic Events 1a and 2 indicarbonated by calcium isotopes. Earth and Planetary Science Letters, 309(1-2):77–88.

Bickle, M. J. (2009). Geological C storage. *Nature Geoscience*, *2*(12), 815-818.

Bond, D. P. and Wignall, P. B. (2014). Large igneous provinces and mass extinctions: an update. Volcanism, impacts, and mass extinctions: causes and effects, 505:29–55.

Brady, P. V. (1991). The effect of silicate weathering on global temperature and atmospheric CO_2. Journal of Geophysical Research: Solid Earth, 96(B11):18101–18106.

Burton, K. W., Gannoun, A., & Parkinson, I. J. (2010). Climate driven glacial–interglacial variations in the osmium isotope composition of seawater recorded by planktic foraminifera. *Earth and Planetary Science Letters*, *295*(1-2), 58-68.

Boutton, T. W. (1991). Stable C isotope ratios of natural materials: 2. Atmospheric, terrestrial, marine, and freshwater environments. In *C isotope techniques*.

Clift, P. D., Wan, S., & Blusztajn, J. (2014). Reconstructing chemical weathering, physical erosion and monsoon intensity since 25 Ma in the northern South China Sea: a review of competing proxies. *Earth-Science Reviews*, *130*, 86-102.

Colbourn, G., Ridgwell, A., and Lenton, T. (2013). The Rock Geochemical Model (RokGeM) v0.9. Geoscientific Model Development, 6(5).

Coogan, L. A., & Gillis, K. M. (2020). The average Phanerozoic CO2 degassing flux estimated from the O-isotopic composition of seawater. *Earth and Planetary Science Letters*, *536*, 116151.

Dickson, A. J., Cohen, A. S., Coe, A. L., Davies, M., Shcherbinina, E. A., & Gavrilov, Y. O. (2015). Evidence for weathering and volcanism during the PETM from Arctic Ocean and Peri-Tethys osmium isotope records. *Palaeogeography, Palaeoclimatology, Palaeoecology*, *438*, 300-307.

Edwards, N. R., & Marsh, R. (2005). Uncertainties due to transport-parameter sensitivity in an efficient 3-D ocean-climate model. *Climate dynamics*, *24*(4), 415-433.

Ernst, R. E. (2014). Large igneous provinces. Cambridge University Press.

Esser, B. K. and Turekian, K. K. (1993). The osmium isotopic composition of the continental crust. Geochimica et Cosmochimica Acta, 57(13):3093–3104.

Fantle, M. S., & Ridgwell, A. (2020). Towards an understanding of the Ca isotopic signal related to ocean acidification and alkalinity overshoots in the rock record. *Chemical Geology*, *547*, 119672.

Foster, G. L., & Rae, J. W. (2016). Reconstructing ocean pH with boron isotopes in foraminifera. *Annual Review of Earth and Planetary Sciences*, *44*, 207-237.

Gales, E., Black, B., and Elkins-Tanton, L. T. (2020). Catites as a record of the C isotope composition of large igneous province outgassing. Earth and Planetary Science Letters, 535:116076.

Gannoun, A., Burton, K. W., Vigier, N., Gíslason, S. R., Rogers, N., Mokadem, F., and Sigfússon, B. (2006). The influence of weathering process on riverine osmium isotopes in a basaltic terrain. Earth and Planetary Science Letters, 243(3-4):732–748.

Georg, R., West, A., Vance, D., Newman, K., and Halliday, A. N. (2013). Is the marine osmium isotope record a probe for CO_2 release from sedimentary rocks? Earth and Planetary Science Letters, 367:28–38.

Goddéris, Y., & François, L. M. (1995). The Cenozoic evolution of the strontium and C cycles: relative importance of continental erosion and mantle exchanges. *Chemical Geology*, *126*(2), 169-190.

Goddéris, Y. and François, L. (1996). Balancing the Cenozoic C and alkalinity cycles: constraints from isotopic records. Geophysical research letters, 23(25):3743–3746.

Goddéris, Y., Donnadieu, Y., Le Hir, G., Lefebvre, V., and Nardin, E. (2014). The role of palaeogeography in the Phanerozoic history of atmospheric CO_2 and climate. Earth-Science Reviews, 128:122–138.

Goldstein, S. L. (1988). Decoupled evolution of Nd and Sr isotopes in the continental crust and the mantle. Nature, 336(6201):733–738.

Griffith, E.M., Fantle, M.S., Eisenhauer, A., Paytan, A. and Bullen, T.D., 2015. Effects of ocean acidification on the marine calcium isotope record at the Paleocene–Eocene Thermal Maximum. *Earth and Planetary Science Letters*, *419*, pp.81-92.

Gutjahr, M., Ridgwell, A., Sexton, P.F., Anagnostou, E., Pearson, P.N., Pälike, H., Norris, R.D., Thomas, E. and Foster, G.L., 2017. Very large release of mostly volcanic C during the Palaeocene–Eocene Thermal Maximum. *Nature*, *548*(7669), pp.573-577.

Hathorne, E. C. and James, R. H.: Temporal record of lithium in seawater: A tracer for silicate weathering?, Earth Planet. Sc. Lett., 246, 393-406, https://doi.org/10.1016/j.epsl.2006.04.020, 2006.

Hodell, D. A., Mead, G. A., and Mueller, P. A. (1990). Variation in the strontium isotopic composition of seawater (8 Ma to present): Implications for chemical weathering rates and dissolved fluxes to the oceans. Chemical Geology: Isotope Geoscience section, 80(4):291–307.

Hodell, D. A., Kamenov, G. D., Hathorne, E. C., Zachos, J. C., Röhl, U., & Westerhold, T. (2007). Variations in the strontium isotope composition of seawater during the Paleocene and early Eocene from ODP Leg 208 (Walvis Ridge). *Geochemistry, Geophysics, Geosystems*, *8*(9).

Holden, P., Edwards, N., Müller, S., Oliver, K., Death, R., and Ridgwell, A. (2013). Controls on the spatial distribution of oceanic $\delta^{13}C_{DIC}$. Biogeosciences, 10(3):1815–1833.

Huh, Y., Chan, L.H., Zhang, L. and Edmond, J.M., 1998. Lithium and its isotopes in major world rivers: implications for weathering and the oceanic budget. *Geochimica et Cosmochimica Acta*, *62*(12), pp.2039-2051.

Jones, C. E. and Jenkyns, H. C. (2001). Seawater strontium isotopes, oceanic anoxic events, and seafloor hydrothermal activity in the Jurassic and Cretaceous. American Journal of Science, 301(2):112–149.

Jones, S.M., Hoggett, M., Greene, S.E. and Dunkley Jones, T., 2019. Large Igneous Province thermogenic greenhouse gas flux could have initiated Paleocene-Eocene Thermal Maximum climate change. *Nature Communications*, *10*(1), pp.1-16.

Kalderon-Asael, B., Katchinoff, J.A., Planavsky, N.J., Hood, A.V.S., Dellinger, M., Bellefroid, E.J., Jones, D.S., Hofmann, A., Ossa, F.O., Macdonald, F.A. and Wang, C., 2021. A lithium-isotope perspective on the evolution of C and silicon cycles. *Nature*, *595*(7867), pp.394-398.

Kamber, B. S. and Petrus, J. A. (2019). The influence of large bolide impacts on earth's C cycle. Elements: An International Magazine of Mineralogy, Geochemistry, and Petrology, 15(5):313–318.

Kelly, D.C., Zachos, J.C., Bralower, T.J. and Schellenberg, S.A., 2005. Enhanced terrestrial weathering/runoff and surface ocean carbonate production during the recovery stages of the Paleocene-Eocene thermal maximum. *Paleoceanography*, *20*(4).

Kender, S., Bogus, K., Pedersen, G.K., Dybkjær, K., Mather, T.A., Mariani, E., Ridgwell, A., Riding, J.B., Wagner, T., Hesselbo, S.P. and Leng, M.J., 2021. Paleocene/Eocene C feedbacks triggered by volcanic activity. *Nature communications*, *12*(1), pp.1-10.

Kirtland Turner, S. and A. Ridgwell, Constraints on the rate of C injection across the PETM – towards a theoretical framework for hyperthermals, EPSL 435, 1-13 (2016).

Kısakűrek, B., James, R. H., and Harris, N. B. (2005). Li and δ^7Li in Himalayan rivers: proxies for silicate weathering? Earth and Planetary Science Letters, 237(3-4):387–401.

Kitch, G. D., Jacobson, A. D., Harper, D. T., Hurtgen, M. T., Sageman, B. B., & Zachos, J. C. (2021). Calcium isotope composition of Morozovella over the late Paleocene–early Eocene. *Geology*, *49*(6), 723-727.

Krabbenhöft, A., Eisenhauer, A., Böhm, F., Vollstaedt, H., Fietzke, J., Liebetrau, V., Augustin, N.,Peucker-Ehrenbrink, B., Müller, M., Horn, C., et al. (2010). Constraining the marine strontium budget with natural strontium isotope fractionations (^{87}Sr/^{86}Sr, $\delta^{88/86}$Sr) of carbonates, hydrothermal solutions and river waters. Geochimica et Cosmochimica Acta, 74(14):4097–4109.

Komar, N., & Zeebe, R. E. (2011). Oceanic calcium changes from enhanced weathering during the Paleocene-Eocene thermal maximum: No effect on calcium-based proxies. *Paleoceanography*, *26*(3).

Kump, L. R. and Arthur, M. A. (1999). Interpreting C-isotope excursions: carbonates and organic matter. Chemical Geology, 161(1-3):181–198.

Le Maitre, R. W., Streckeisen, A., and Zanettin, B. (2004). Igneous rocks: IUGS classification and glossary: recommendations of the International Union of Geological Sciences, Subcommission on the Systematics of Igneous Rock. University of Cambridge.

Lechler, M., von Strandmann, P. A. P., Jenkyns, H. C., Prosser, G., and Parente, M. (2015). Lithium-isotope evidence for enhanced silicate weathering during OAE 1a (Early Aptian Selli event). Earth and Planetary Science Letters, 432:210–222.

Li, G., Chen, J., Ji, J., Liu, L., Yang, J. and Sheng, X., 2007. Global cooling forced increase in marine strontium isotopic ratios: Importance of mica weathering and a kinetic approach. *Earth and Planetary Science Letters*, *254*(3-4), pp.303-312.

Lord, N. S., Ridgwell, A., Thorne, M. C., & Lunt, D. J. (2016). An impulse response function for the "long tail" of excess atmospheric CO2 in an Earth system model. *Global Biogeochemical Cycles*, *30*(1), 2-17.

Lu, X., Kendall, B., Stein, H. J., and Hannah, J. L.: Temporal record of osmium concentrations and 187Os/188Os in organic-rich mudrocks: Implications for the osmium geochemical cycle and the use of osmium as a paleoceanographic tracer, Geochim. Cosmochim. Ac., 216, 221–241, https://doi.org/10.1016/j.gca.2017.06.046, 2017.

Lunt, D.J., Ridgwell, A., Sluijs, A., Zachos, J., Hunter, S. and Haywood, A., 2011. A model for orbital pacing of methane hydrate destabilization during the Palaeogene. *Nature Geoscience*, *4*(11), pp.775-778.

McCabe, G.J. and Wolock, D.M., 2013. Temporal and spatial variability of the global water balance. *Climatic Change*, *120*(1), pp.375-387.

McInerney, F. A. & Wing, S. L. The Paleocene–Eocene Thermal Maximum: a perturbation of C cycle, climate, and biosphere with implications for the future. *Annu. Rev. Earth Planet. Sci.* 39, 489–516 (2011)

Michel, J., Laugié, M., Pohl, A., Lanteaume, C., Masse, J. P., Donnadieu, Y., & Borgomano, J. (2019). Marine carbonate factories: a global model of carbonate platform distribution. *International Journal of Earth Sciences*, *108*(6), 1773-1792.

Miller, C.A., Peucker-Ehrenbrink, B. and Schauble, E.A., 2015. Theoretical modeling of rhenium isotope fractionation, natural variations across a black shale weathering profile, and potential as a paleoredox proxy. *Earth and Planetary Science Letters*, *430*, pp.339-348.

Mills, B., Daines, S. J., and Lenton, T. M. (2014). Changing tectonic controls on the long-term C cycle from Mesozoic to present. Geochemistry, Geophysics, Geosystems, 15(12):4866–4884.

Mills, B. J., Scotese, C. R., Walding, N. G., Shields, G. A., and Lenton, T. M. (2017). Elevated CO_2 degassing rates prevented the return of Snowball Earth during the Phanerozoic. Nature communications, 8(1):1–7.

Misra, S. and Froelich, P. N. (2012). Lithium isotope history of Cenozoic seawater: changes in silicate weathering and reverse weathering. Science, 335(6070):818–823.

Monteiro, F., Pancost, R., Ridgwell, A., and Donnadieu, Y. (2012). Nutrients as the dominant control on the spread of anoxia and euxinia across the Cenomanian-Turonian oceanic anoxic event (OAE2): Model-data comparison. Paleoceanography, 27(4).

Mook, W. G., Bommerson, J. C., & Staverman, W. H. (1974). C isotope fractionation between dissolved bicarbonate and gaseous C dioxide. *Earth and planetary science letters*, *22*(2), 169-176.

Nance, R. D., Murphy, J. B., & Santosh, M. (2014). The supercontinent cycle: a retrospective essay. *Gondwana Research*, *25*(1), 4-29.

Papadomanolaki, N.M., Sluijs, A. and Slomp, C.P., 2022. Eutrophication and deoxygenation forcing of marginal marine organic C burial during the PETM. *Paleoceanography and Paleoclimatology*, *37*(3), p.e2021PA004232.

Paytan et al., 2021: A 35 Myr Record of Seawater Stable Sr Isotopes Reveals a Fluctuating Global C Cycle

Pearce, C. R., Parkinson, I. J., Gaillardet, J., Charlier, B. L., Mokadem, F., and Burton, K. W. (2015). Reassessing the stable ($\delta^{88/86}$Sr) and radiogenic (^{87}Sr/^{86}Sr) strontium isotopic composition of marine inputs. Geochimica et Cosmochimica Acta, 157:125–146.

Pegram, W.J., Krishnaswami, S., Ravizza, G.E. and Turekian, K.K., 1992. The record of sea water 187Os/186Os variation through the Cenozoic. *Earth and Planetary Science Letters*, *113*(4), pp.569-576.

Penman, D. E., Rugenstein, J. K. C., Ibarra, D. E., and Winnick, M. J. (2020). silicate weathering as a feedback and forcing in Earth's climate and C cycle. Earth-Science Reviews, page 103298.

Pogge von Strandmann, P. A., Jenkyns, H. C., and Woodfine, R. G. (2013). Lithium isotope evidence for enhanced weathering during Oceanic Anoxic Event 2. Nature Geoscience, 6(8):668–672.

Pogge von Strandmann, P. A. , Kasemann, S. A., & Wimpenny, J. B. (2020). Lithium and lithium isotopes in Earth's surface cycles. *Elements: An International Magazine of Mineralogy, Geochemistry, and Petrology*, *16*(4), 253-258.

Pogge von Strandmann, P.A., Jones, M.T., West, A.J., Murphy, M.J., Stokke, E.W., Tarbuck, G., Wilson, D.J., Pearce, C.R. and Schmidt, D.N., 2021. Lithium isotope evidence for enhanced weathering and erosion during the Paleocene-Eocene Thermal Maximum. *Science advances*, *7*(42), p.eabh4224.

Pohl, A., Donnadieu, Y., Godderis, Y., Lanteaume, C., Hairabian, A., Frau, C., Michel, J., Laugie, M., Reijmer, J. J., Scotese, C. R., et al. (2020). carbonate platform production during the Cretaceous. Geological Society of America Bulletin.

Raymo, M. E., Ruddiman, W. F., & Froelich, P. N. (1988). Influence of late Cenozoic mountain building on ocean geochemical cycles. *Geology*, *16*(7), 649-653.

Ravizza, G., Norris, R., Blusztajn, J., and Aubry, M.-P. (2001). An osmium isotope excursion associated with the late Paleocene thermal maximum: Evidence of intensified chemical weathering. Paleoceanography, 16(2):155–163.

Reijmer, J. J. (2021). Marine carbonate factories: Review and update. *Sedimentology*, *68*(5), 1729-1796.

Reynolds, P., Planke, S., Millett, J.M., Jerram, D.A., Trulsvik, M., Schofield, N. and Myklebust, R., 2017. Hydrothermal vent complexes offshore Northeast Greenland: A potential role in driving the PETM. *Earth and Planetary Science Letters*, *467*, pp.72-78.

Richter, F. M., Rowley, D. B., & DePaolo, D. J. (1992). Sr isotope evolution of seawater: the role of tectonics. *Earth and Planetary Science Letters*, *109*(1-2), 11-23.

Ridgwell, A., Hargreaves, J., Edwards, N. R., Annan, J., Lenton, T. M., Marsh, R., Yool, A., and Watson, A. (2007a). Marine geochemical data assimilation in an efficient Earth System Model of global biogeochemical cycling. Biogeosciences, 4(1):87–104.

Ridgwell, A., I. Zondervan, J. Hargreaves, J. Bijma, and T. Lenton (2007b). Assessing the potential long-term increase of oceanic fossil fuel CO2 uptake due to 'CO2-calcification feedback', Biogeosciences 4, 481-492.

Ridgwell, A. and Hargreaves, J. (2007). Regulation of atmospheric CO_2 by deep-sea sediments in an Earth system model. Global Biogeochemical Cycles, 21(2).

Sano, T. and Nishio, Y. (2015). Lithium isotopic evidence for magmatic assimilation of hydrothermally influenced crust beneath oceanic large igneous provinces. The Origin, Evolution, and Environmental Impact of Oceanic Large Igneous Provinces. Geol. Soc. Amer. Spec. Pub, 511:173–183.

Sarmiento, J. L. (2013). *Ocean biogeochemical dynamics*. Princeton University Press.

Seyfried Jr, W. E. and Mottl, M. J. (1982). Hydrothermal alteration of basalt by seawater under seawater-dominated conditions. Geochimica et Cosmochimica Acta, 46(6):985–1002.

Staudigel, H. (2003). Hydrothermal alteration processes in the oceanic crust. *Treatise on geochemistry*, *3*, 659.

Svensen, H. H., Jerram, D. A., Polozov, A. G., Planke, S., Neal, C. R., Augland, L. E., and Emeleus,

H. C. (2019). Thinking about LIPs: A brief history of ideas in Large igneous province research. Tectonophysics, 760:229–251.

Taylor, L. L., Quirk, J., Thorley, R. M., Kharecha, P. A., Hansen, J., Ridgwell, A., ... & Beerling, D. J. (2016). Enhanced weathering strategies for stabilizing climate and averting ocean acidification. *Nature Climate Change*, *6*(4), 402-406.

Tejada, M., Mahoney, J., Castillo, P., Ingle, S., Sheth, H., and Weis, D. (2004). Pin-pricking the elephant: Evidence on the origin of the Ontong Java Plateau from Pb-Sr-Hf-Nd isotopic characteristics of ODP Leg 192 basalts. Geological Society, London, Special Publications, 229(1):133–150.

Tejada, M. L. G., Suzuki, K., Kuroda, J., Coccioni, R., Mahoney, J. J., Ohkouchi, N., Sakamoto, T., and Tatsumi, Y. (2009). Ontong Java Plateau eruption as a trigger for the early Aptian oceanic anoxic event. Geology, 37(9):855–858.

Tejada, M., Suzuki, K., Hanyu, T., Mahoney, J., Ishikawa, A., Tatsumi, Y., Chang, Q., and Nakai, S.(2013). Cryptic lower crustal signature in the source of the Ontong Java Plateau revealed by Os and Hf isotopes. Earth and Planetary Science Letters, 377:84–96.

Thomas, D.J. and Bralower, T.J., 2005. Sedimentary trace element constraints on the role of North Atlantic Igneous Province volcanism in late Paleocene–early Eocene environmental change. *Marine Geology*, *217*(3-4), pp.233-254.

Tipper, E. T., Galy, A., and Bickle, M. J. (2008). Calcium and magnesium isotope systematics in rivers draining the Himalaya-Tibetan-Plateau region: Lithological or fractionation control? Geochimica et Cosmochimica Acta, 72(4):1057–1075.

Tréguer, P.J. and De La Rocha, C.L., 2013. The world ocean silica cycle. *Annual review of marine science*, *5*, pp.477-501.

Turchyn, A. V. and DePaolo, D. J. (2019). Seawater Chemistry through Phanerozoic Time. Annual Review of Earth and Planetary Sciences, 47:197–224.

Turgeon, S. C., & Creaser, R. A. (2008). Cretaceous oceanic anoxic event 2 triggered by a massive magmatic episode. *Nature*, *454*(7202), 323-326.

Vervoort, P., Adloff, M., Greene, S., and Turner, S. K. (2019). Negative C isotope excursions: an interpretive framework. Environmental Research Letters, 14(8):085014.

Wieczorek, R., Fantle, M. S., Kump, L. R., & Ravizza, G. (2013). Geochemical evidence for volcanic activity prior to and enhanced terrestrial weathering during the Paleocene Eocene Thermal Maximum. *Geochimica et Cosmochimica Acta*, *119*, 391-410.

Zhang, J., Quay, P. D., & Wilbur, D. O. (1995). C isotope fractionation during gas-water exchange and dissolution of CO2. *Geochimica et Cosmochimica Acta*, *59*(1), 107-114.